RSC Sustainability

ROYAL SOCIETY OF CHEMISTRY

TUTORIAL REVIEW

View Article Online
View Journal

Cite this: DOI: 10.1039/d6su00010j

Analysis of emerging PFAS contaminants in water: review and future perspectives

Baljit Singh, *[abcd] Zina Fredj,[e] Rangasamy Savitha,[d] Abhijnan Bhat, [bcd] Gayathree Thenuwara,[cd] Isha Dahiya,[f] Suneha Goswami, [f] Simrjit Singh[g] and Xolile Fuku [h]

Per- and polyfluoroalkyl substances (PFAS) are widely used in numerous industrial and consumer products. These compounds exhibit remarkable environmental persistence which allows them to accumulate in ecosystems and pose serious risks to water quality, the environment and human health, thereby underscoring the urgent need for effective monitoring and control. To mitigate the long-term impacts of PFAS contamination, robust and reliable advanced analytical methods and sensor technologies are essential. This review critically examines current analytical methods, including coupled chromatographic techniques, emerging sensor-based (optical and electrochemical sensors) methods and separation-based electrophoresis for PFAS detection. Recent progress in device miniaturisation coupled with integration of Internet of Things (IoT), artificial intelligence (AI), and machine learning (ML), has substantially strengthened the potential of these methods for real-time monitoring and advanced environmental management. Significant emphasis is placed on recent advancements in the development of sensors and methods capable of detecting the broader structural diversity of PFAS, key challenges, and future directions that highlight potential innovations. Timely PFAS detection and granular data collection can help in protecting global communities by bridging the gap between environmental surveillance and public safety.

Received 6th January 2026
Accepted 31st May 2026

DOI: 10.1039/d6su00010j

rsc.li/rscsus

Sustainability spotlight

PFAS contamination poses a serious threat to global water quality and human health. This review examines current analytical approaches including chromatographic techniques, emerging optical and electrochemical sensors, and electrophoretic methods for PFAS detection. It highlights recent progress in developing sensors and methods that can detect the broader structural diversity of PFAS, associated challenges, and future directions. Advancements such as multiplexed and hybrid systems, sustainable fabrication methods, and standardisation of regulatory systems, support more reliable PFAS monitoring. The timely processing and dissemination of PFAS data will help close the gap between environmental surveillance and public safety.

1. Introduction

Per- and polyfluoroalkyl substances (PFAS) are a large and chemically diverse group of synthetic compounds that have become a major environmental and public health concern. Sustained exposure to PFAS has been associated with a range of adverse outcomes, including immune suppression, endocrine disruption, developmental toxicity, and an increased risk of certain cancers.[1–3] Their widespread industrial and commercial applications, combined with exceptional resistance to chemical and biological degradation, have contributed to their global accumulation and potential toxicity.[1] Chemically, PFAS consist of aliphatic molecules that contain one or more perfluoroalkyl groups (C_nF_{2n+1}).[4] Depending on the functional groups, these compounds can exist as anionic, cationic, or zwitterionic species and may occur in linear, branched, or cyclic molecular forms.[5]

The key structural feature of PFAS is the carbon–fluorine (C–F) bond, one of the strongest bonds known in organic chemistry, which provides extraordinary thermal and chemical stability.[6] This remarkable durability has led to PFAS being widely referred as 'forever chemicals'.[7] PFAS possess both hydrophobic and lipophobic properties, allowing them to move through environmental media such as air, water, soil, and living organisms.[8–10] Due

[a]MiCRA Biodiagnostics Technology Gateway, Technological University Dublin (TU Dublin), Dublin, D24 FKT9, Ireland. E-mail: baljit.singh@tudublin.ie; Tel: +353 1 220 7863
[b]Health, Engineering and Materials Science Research Hub, Technological University Dublin (TU Dublin), Dublin, D24 FKT9, Ireland
[c]Nanolab Research Centre, Physical to Life Sciences Research Hub, Technological University Dublin (TU Dublin), Dublin, D08 CKP1, Ireland
[d]School of Food Science and Environmental Health, Technological University Dublin (TU Dublin), Grangegorman, Dublin, D07 H6K8, Ireland
[e]Faculty of Engineering, Free University of Bozen-Bolzano, Italy
[f]Division of Biochemistry, ICAR-Indian Agricultural Research Institute, New Delhi-110012, India
[g]Nanotechnology Centre, Centre for Energy and Environmental Technologies, VSB-Technical University of Ostrava, 17. listopadu, Ostrava, 70800, Czech Republic
[h]Institute for Nanotechnology and Water Sustainability (iNanoWS), College of Science, Engineering, and Technology, University of South Africa, FL 1710, South Africa

to these distinctive physicochemical properties, PFAS have been widely used in numerous industrial and consumer products. Typical applications include firefighting foams, nonstick cookware, food packaging, lubricants, water-repellent textiles, and coated fabrics.[11] The United States Environmental Protection Agency (US EPA) estimates that more than 12 000 individual PFAS structures are currently in production and use.[12] Historically, perfluorooctanesulfonate (PFOS), perfluorooctanoic acid (PFOA), and perfluorohexanesulfonate (PFHxS) have been the most extensively studied and regulated members of this group. In response to restrictions on these long-chain PFAS, manufacturers have shifted toward short-chain analogues such as perfluorobutanoic acid (PFBA), perfluorobutane sulfonic acid (PFBS), and newer replacement chemistries like GenX.[13–15] More recently, ultra-short-chain PFAS (C2–C3) have been identified in several environmental matrices, raising additional concerns regarding their persistence and mobility.[14]

The large-scale manufacturing and extensive application of PFAS have led to their global widespread presence in surface waters, groundwater, sediments, and biological systems. Even at nanomolar concentrations, compounds such as PFOS and PFOA can persist through trophic transfer and accumulate in human tissues.[16] In particular, PFOS has been shown to impair thyroid hormone regulation, suppress immune function, and cause reproductive and developmental toxicity in aquatic organisms and mammals.[17,18] In aquatic environments, PFOS bioaccumulates through the food chain, with fish and invertebrates serving as key exposure vectors to higher trophic levels including humans.[19,20] Its persistence and lipophilic character facilitate accumulation in the liver, kidney, and blood serum, where it has been associated with altered lipid metabolism and hepatotoxicity.[21] The U.S. Agency for Toxic Substances and Disease Registry (ATSDR) has recognised the broader class of PFAS compounds as posing significant toxicological hazards. Under the Stockholm Convention, several PFAS compounds have been formally listed as persistent organic pollutants (POPs): PFOS in 2009, PFOA in 2019, and PFHxS in 2022, with measures adopted to address their production and use.[22–25]

The exceptional strength of the C–F bond and the surfactant-like nature of PFAS pose major challenges for conventional chemical and biological treatment processes. In aqueous environments, PFAS molecules often self-assemble into micellar aggregates or form interfacial films that impede adsorption and separation, complicating analytical and removal strategies.[16] Accurate detection has become a central component of PFAS remediation efforts. The capability to identify pre-existing and emerging PFAS at ultra-trace concentrations is crucial for environmental surveillance, risk assessment, and the implementation of regulatory measures.[26] Recent research highlights the growing demand for rapid and cost-effective analytical systems that offer high sensitivity and selectivity.[27] These challenges have driven the development of advanced sensing technologies designed to facilitate near real-time PFAS monitoring across diverse environmental matrices.[13,14]

PFAS detection has traditionally relied on chromatographic techniques coupled with mass spectrometry, including liquid chromatography-mass spectrometry (LC-MS) and gas chromatography-mass spectrometry (GC-MS).[28,29] These analytical tools provide excellent sensitivity and molecular precision for a wide range of ionic and semi-volatile PFAS. However, their application remains largely limited to sophisticated laboratory environments because they require extensive sample preparation, costly instrumentation, and skilled personnel.[30–32] Long analysis times, high operational costs, and dependence on complex laboratory facilities can delay timely data generation and hinder rapid decision-making.[31,32] Although these chromatographic methods continue to represent the benchmark for analytical accuracy, the lack of portability restricts their suitability for field deployment and routine environmental surveillance, which are increasingly important for remote water quality assessment.[33]

Another common analytical approach is traditional colorimetry, in which a chromogenic indicator is used to produce a response signal (often a visible colour change) upon exposure to the analyte of interest. The distinctive chemical nature of PFAS, including their strong C–F bonds, absence of inherent chromophores, and exceptional molecular stability, limits the effectiveness of traditional colorimetric and derivatisation-based analytical approaches.[16] Additionally, interference from co-existing environmental matrices can complicate quantitative analysis.[34] In response to these challenges, increasing attention has been given towards sensor-based detection technologies capable of providing rapid, sensitive, and selective PFAS measurements at trace concentrations. Optical and electrochemical sensors are emerging as valuable alternatives to conventional laboratory techniques.[26,35–37] Recent progress in device miniaturisation, coupled with integration of Internet of Things (IoT), artificial intelligence (AI), and machine learning (ML), has substantially strengthened the potential of these sensors for continuous, real-time monitoring and advanced environmental management. These digital tools enable automated anomaly detection, predictive modelling, and data-driven decision-making.[36]

While considering analytical and practical constraints, Section 2 provides an overview of coupled chromatographic detection methods, with emphasis on their analytical performance, significance, and the limitations that arise in large-scale or real-time monitoring. Subsequently, Sections 3 and 4 explore sensor-based detection technologies and recent developments, while Section 5 examines electrophoresis as a separation-coupled analytical approach. The discussion also covers persistent challenges such as matrix interferences, the detection of previously unrecognised PFAS, and the lack of standardised analytical protocols. Finally, the review outlines future research priorities (Section 6) aimed at enhancing the efficiency, sensitivity, and overall practicality of PFAS detection across diverse and complex environmental matrices.[26,27,37,38]

2. Chromatographic techniques for PFAS analysis

PFAS can exist in anionic, cationic, and zwitterionic forms, resulting in variations in charge, polarity, and functional groups

that complicate simultaneous detection of multiple PFAS classes using a single standard analytical approach. Furthermore, PFAS comprise thousands of diverse chemicals, which include perfluoroalkyl carboxylic acids, perfluorosulfonic acids, fluorotelomer compounds, and other emerging alternatives. These chemicals have unique differences including their chain lengths, hydrophobicities, and ionisation states. Therefore, it is worth noting that chromatography coupled with mass spectrometry (*e.g.* LC-MS and LC-MS/MS), is the dominant, accurate and sensitive approach that is used for PFAS identification and monitoring, especially in water, soil, biota, and human samples (Fig. 1, Top).[11] To address the challenge of detecting structurally diverse PFAS across different ionic classes, a range of complementary chromatographic methods has been employed, including LC-MS, LC-MS/MS, GC-MS, HPLC, UHPLC, and CLC.

LC-MS is one of the most effective PFAS analytical techniques for various environmental samples, offering limits of detection (LODs) in the nanogram range. LC-MS/MS is regarded as the gold standard due to its superior sensitivity for PFAS detection.[28] A method-specific LOD for LC-MS/MS reaching 0.1 ng L^{-1} was reported,[29] enabling precise quantification of priority analytes such as PFOA and PFOS. The US EPA lists drinking-water limits of 0.4 μg L^{-1} and 0.2 μg L^{-1} for PFOA and PFOS, respectively.[38] In drinking-water analysis, the monitoring practices primarily rely on HPLC-MS/MS. The US EPA has published three validated drinking-water analytical methods – Methods 537, 537.1 and 533 to support consistent and reliable monitoring of PFAS.

Method 537 (Ver. 1.1, 2009) targets a defined list of legacy long-chain PFAS in drinking water using solid-phase extraction (SPE) followed by LC-MS/MS. Method 537.1 (first published in 2018, updated in 2020) expands the list to include additional PFAS, including some shorter-chain 'replacement' compounds, while retaining SPE/LC-MS/MS. Method 533 (2019) further broadens the scope to include a number of ultra-short and short-chain PFAS analytes, employs a weak anion-exchange polymeric SPE, and uses isotope-dilution LC-MS/MS for enhanced quantification accuracy. When used together, Methods 537.1 and 533 provide complementary analyte coverage, allowing measurement of about 29 PFAS compounds in drinking water.[31,40] The isotope-dilution approach enhances analytical precision by compensating for matrix interferences, instrumental variability, and sample losses, thereby improving reproducibility and quantification reliability.[30,31]

A persistent challenge in PFAS chromatographic analysis is the speciation of structurally similar congeners, particularly branched and linear isomers of the same compound. PFOS and PFOA, for instance, each exists as mixtures of linear and branched isomers that share identical molecular masses and thus cannot be resolved based on mass alone. Reversed-phase LC exploits subtle differences in hydrophobicity between isomers, with linear isomers typically eluting slightly later than their branched counterparts due to stronger hydrophobic interactions with the stationary phase; however, co-elution remains frequent for complex environmental mixtures. To overcome this, ion mobility spectrometry (IMS) has been hyphenated with LC-QTOF-MS, adding a gas-phase separation dimension based on collision cross-section (CCS) values that are distinctive for each isomer.

Using Structures for Lossless Ion Manipulations (SLIM)-based high-resolution IMS, PFOS and PFHxS branched isomers have been resolved with CCS differences as small as 0.5% (a resolution unattainable by chromatography alone). Complementary tandem MS fragmentation (MS/MS) provides additional structural differentiation through class-specific neutral losses and diagnostic fragment ions, thereby enabling unambiguous isomer assignment even when mobility separation is incomplete. For anionic PFAS species, matrix co-extractants, particularly natural organic matter, humic acids, and co-occurring surfactants can cause ion suppression during electrospray ionisation, leading to systematic underestimation of concentrations. Isotope-dilution using mass-labelled internal standards (*e.g.*, $^{13}C_4$-PFOA and $^{13}C_8$-PFOS) is the principal strategy to correct for these matrix-induced signal suppression effects, compensating for both variable extraction recoveries and ionisation interference in complex water matrices.[41,42]

LC- and GC-based approaches coupled with MS offer high sensitivity, accuracy, and selectivity. For instance, UHPLC combined with high-resolution accurate mass spectrometry (HRAM), particularly Orbitrap MS, has been employed for PFAS determination. This combination achieved recoveries above 90% for cationic and zwitterionic PFAS but only about 12% for anionic species, thereby highlighting the need for further optimisation.[43] In this regard, Coggan *et al.* developed an LC-MS/MS method to quantify 53 legacy and emerging PFAS, using solid-phase extraction for sample preparation.[44] Applied to aqueous matrices, the method achieved an LOD of 0.28–18 ng L^{-1} and limits of quantitation (LOQ) of 0.35–26 ng L^{-1}.[44] Extending targeted surveillance to consumer products, Chow *et al.* assessed PFAS occurrence in 101 uniquely labelled bottled-water products in the United States and quantified 32 PFAS by SPE-LC-MS/MS (Fig. 1, bottom).[39]

To move beyond fixed target lists and support structural elucidation, de Vega *et al.* combined UHPLC, ion-mobility spectrometry, and QTOF-MS, integrating drift time, collision cross-section, accurate mass, mass defects, and fragmentation; the targeted workflow validated 14 sulfonated PFAS by MS/MS, while non-targeted screening flagged fluorinated features *via* mass-defect and neutral-loss filters followed by diagnostic fragments.[45] Recognising the need to capture very short-chain species, ultra-short-chain PFAS (C2–C3) were detected in AFFF-impacted groundwater, river water, and rainwater using LC-QTOF-MS and ultra-performance convergence chromatography (UPC^2) coupled to MS/MS in negative electrospray mode, achieving on-column LODs as low as 0.4 pg for trifluoroacetate, with narrow peak widths of 3–6 seconds, and total run times of approximately 8 minutes.[46,47] For routine monitoring where sensitivity and speed are critical, Mulabagal *et al.* (2018) reported a UHPLC-MS/MS method for 23 PFAS in estuarine water with a LOD of 0.48–1.68 pg per injection and LOQ of 1.71–5.40 pg per injection.[48] In parallel, an HLB-WAX/PAN solid-phase microextraction coating evaluated in combination with UHPLC-MS/MS using laminar-flow technology delivered limits of quantitation of 2.5 ng L^{-1} for PFOS and 1 ng L^{-1} for GenX,

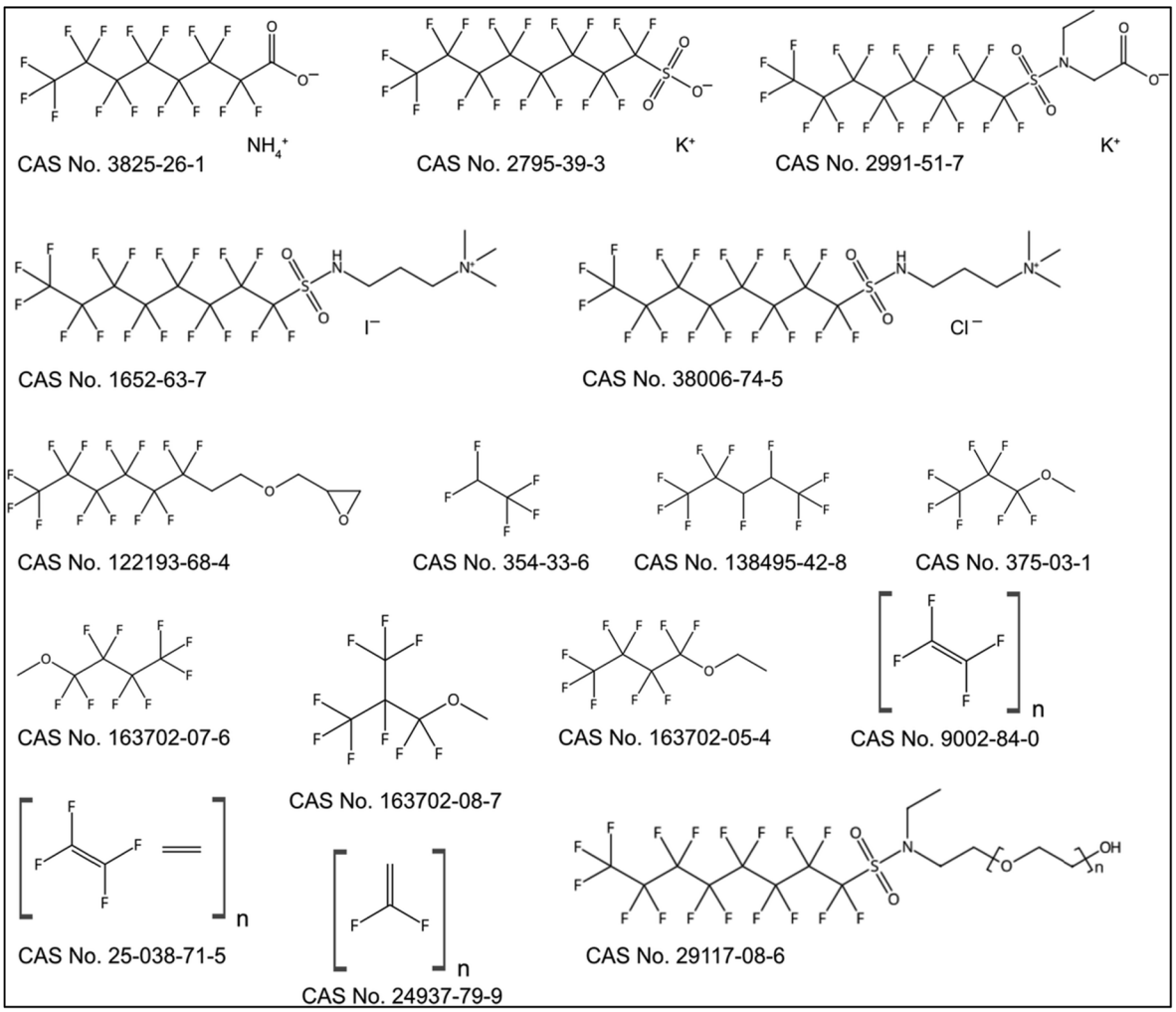

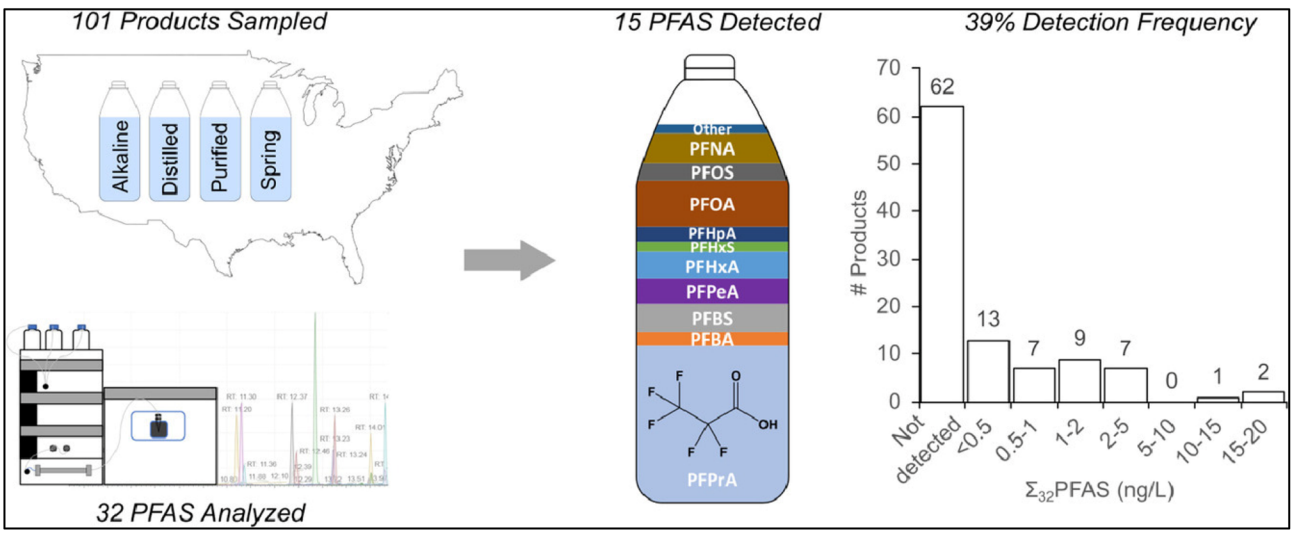

Fig. 1 Top: Structures and CAS numbers of the PFAS with more than 10 assigned uses.[11] Reproduced from ref. 11 Copyright (2020) The Royal Society of Chemistry under a Creative Commons Attribution-NonCommercial 3.0 Unported Licence (CC BY-NC 3.0). Bottom: Graphical abstract: Detection of ultrashort-chain and other per- and polyfluoroalkyl substances (PFAS) in U.S. bottled water.[39] Reproduced from ref. 39 Copyright (2021) with permission from Elsevier.

Table 1 Chromatographic methods for PFAS detection in various water samples

Analyte(s)	Sample type	Extraction/pretreatment	Analytical technique/ method	Detection limits (LOD/LOQ)	Ref.
19 PFAS: 13 PFCAs (PFBA → PFOcDA), 4 PFSAs (PFBS, PFHxS, PFOS, PFDS), FOSA & FOSAA	River, coastal wastewater & WWTP effluents; Bohai Sea basin, China; 1 L per sample	SPE (Waters Oasis HLB, 200 mg); GFF prefilter (1.6 μm); 2 ng IS spike; eluted 4 mL MeOH + 4 mL 0.1% NH_4OH/MeOH; reconstituted in 1 mL MeOH	HPLC-ESI(−)-MS/MS; Agilent 1200 + 6410 QqQ; Eclipse Plus C_{18} (100 × 2.1 mm, 3.5 μm); 10 mM NH_4Ac/MeOH gradient; MRM; IS calibration	LOQ: 0.04–0.22 ng L^{-1}	14
PFBA, PFPeA, PFHxA, PFHpA, PFOA, PFNA, PFDA, PFUnA, PFBS, PFHxS, and PFOS	Laboratory batch sorption solutions (artificial groundwater) & soil extracts	Direct injection (aqueous phase); solvent extraction (solid phase)	LC-MS/MS (AB Sciex API 3200, TQ)	LOQ: 0.02–0.5 ng g^{-1} (soil); 2–9 ng L^{-1} (aqueous)	16
23 PFAS (13 PFCAs, 8 PFSAs & 2 short-chain perfluoroethers)	Estuarine water (surface water, 16 locations in the Perdido Bay estuary)	Filtration (0.7 μm GF/C glass microfiber filter) + SPE (Oasis PRiME HLB, 6 cc, 200 mg; 4 L sample)	UHPLC-MS/MS (triple quadrupole, MRM)	LOD: 0.48–1.68 pg per injection; LOQ: 1.71–5.40 pg per injection	48
PFAS (26 newly-identified + 21 legacy)	AFFF formulations + groundwater (U.S. military bases)	AFFF: methanol dilution (100 000–100 000 00×); groundwater: micro-LLE (3 mL sample, 1.7 mL extractant), non-aqueous LVI (900 μL injection)	HPLC-MS/MS (orthogonal Sil + NH_2 guard columns + C_{18}; ESI; TQ)	MDL: 0.71–67 ng L^{-1}	50
10 PFCs: 7 PFCAs (PFBA, PFPeA, PFHxA, PFHpA, PFOA, PFNA, and PFDA) + 3 PFSAs (PFBS, PFHxS, and PFOS)	Raw and treated drinking water (surface water & groundwater; 331 raw + 110 treated samples; 100 French departments)	Automated offline SPE (Oasis WAX, 6 cm^3/150 mg; Gilson ASPEC GX-274); 500 mL sample; eluted with 2 mL MeOH + 4 mL 0.1% NH_4OH in MeOH; final volume 200 μL	LC-MS/MS (Thermo TSQ Quantum Ultra; negative ESI; MRM)	LOD: ∼1.3 ng L^{-1}; LOQ: 2 ng L^{-1} for PFOA; LOQ: 4 ng L^{-1} (all compounds)	53
PFOS and PFOA	Surface water (Xiangjiang river, China; filtered through a 0.45 μm membrane)	Mixed-mode SPME fiber (APTES + C18-TMOS sol–gel on anodized TiO_2 nanotube/Ti wire); 20 mL sample; 60 min immersion at pH 2.0; desorption in 100 μL MeOH for 15 min	LC–ESI-MS (single quadrupole, Waters ZQ4000; negative mode; SIR at *m*/*z* 499 for PFOS, 369 for PFOA; XB-C_{18} column)	LOD: 2.5 pg mL^{-1} (PFOS), 7.5 pg mL^{-1} (PFOA)	54
6 PFCs: PFHA, PFOA, PFOS, PFDA, PFDoA, and PFTA	Surface water (Xiangjiang river, China); filtered through a 0.45 μm cellulose membrane; stored in amber glass bottles at 4 °C	Direct-immersion SPME using novel PIL-POSS fiber (crosslinked polymeric ionic liquid + POSS on anodized TiO_2/Ti wire); 25 mL sample; pH 2.0; 25% NaCl (w/v); 60 min extraction; desorption in 150 μL MeOH for 5 min (×3); 10 μL injected	HPLC-ESI-MS/MS (Agilent 1290/Agilent 6460 QQQ; negative MRM mode; Unitary C_{18} column 150 × 2.1 mm, 2.8 μm; mobile phase: ACN/10 mM ammonium acetate; flow rate 0.3 mL min^{-1})	LOD: 0.005–0.08 ng mL^{-1} (analyte-dependent)	55

Table 1 (*Contd.*)

Analyte(s)	Sample type	Extraction/pretreatment	Analytical technique/ method	Detection limits (LOD/LOQ)	Ref.
8 PFCs: PFBA, PFHxA, PFOA, PFNA, PFDA, PFBS, PFHxS, and PFOS	Lake water, river water, whole blood, and milk (China)	SPME *via* a surface-coated wooden-tip probe (birch tip silanized with C18-quaternary ammonium; dual reversed-phase + ion-exchange adsorption); ≥1 mL sample; direct ESI induction from tip post-extraction; no chromatographic separation; 4000–8000× enrichment (water), 100–500× (blood/milk)	SPME-AMS; ESI negative mode; isotope IS or isotope dilution calibration; Orbitrap or QQQ MS	LOD: 0.06–0.59 ng L^{-1} LOQ: 0.21–1.98 ng L^{-1}	56
11 PFAAs: PFHxA, PFHpA, PFOA, PFNA, PFDA, PFUnDA, PFDoDA, PFHxS, br-PFOS, L-PFOS, and PFDS	Rain, snowmelt, streamwater; 2 pristine boreal catchments, Krycklan, N. Sweden (2011–2012)	PP funnel + HDPE bottle (rain); 1.44 m^2 lysimeter (snowmelt); grab samples (streams); 0.45 μm GFF filtration; large-volume SPE; PEEK tubing + waters PFC-kit trapping column; procedural blanks per batch; fluoropolymer materials avoided	UPLC-MS/MS; ESI negative MRM; ^{13}C-labelled IS per analyte; Waters PFC-kit between pump and injector	LOD: deposition: 3–97 pg L^{-1} (analyte-dependent); streams: 5–320 pg L^{-1} (analyte-dependent)	57
14 volatile PFAS: PFHxI, PFOI, 4 : 2 FTI, 6 : 2 FTI, 8 : 2 FTI, 6 : 2 FTOH, 8 : 2 FTOH, 10 : 2 FTOH, 6 : 2 FTAC, 8 : 2 FTAC, 6 : 2 FTMAC, 8 : 2 FTMAC, MeFOSA, and EtFOSA	Tap water, industrial effluents, WWTP inlet/ outlet, and sediments (France)	Water: HS-SPME (DVB/ CAR/PDMS fiber; 50 °C, 35 min; 5 mL + NaCl); sediment: HS-SPME (0.5 g dw + 3 mL Milli-Q + NaCl; 70 °C, 45 min); validated per SANTE 11945/2015	GC/MS; DB-5 column; EI-SIM mode	LOQ: water: 20–100 ng L^{-1}; sediment: 1–3 ng g^{-1} dw	58
18 PFAS: PFBA, PFPeA, PFHxA, PFHpA, PFOA, PFNA, PFDA, PFUnDA, PFDoDA, PFTrDA, PFTeDA, PFBS, PFHxS, PFHpS, PFOS, PFDS, FOSA, and EtFOSAA	WWTP influents/effluents/ dewatered sludge (×3); DWTP influents/effluents/ tap water (×2); river source waters (Beijiang, Zhujiang, Dongjiang, Xijiang); Guangzhou, China (2014–2015); 24 h composites	Water (500 mL): GFF filtration + SPE (Oasis WAX); eluted with MeOH + 0.1% NH_4OH/MeOH; reconstituted in 0.5 mL MeOH; sludge (1 g dw): ultrasonic extraction (acetic acid + MeOH; 60 °C) + WAX SPE cleanup	HPLC-MS/MS; Agilent 1200 + 6460 QQQ; ESI negative MRM; Betasil C_{18} (2.1 × 50 mm, 5 μm); ^{13}C/^{18}O-IS per analyte	LOD: 0.02–0.10 ng L^{-1} for water, 0.02–0.04 ng g^{-1} for sludge; LOQ: 0.06–0.33 ng L^{-1} for water, 0.066–0.14 ng g^{-1} for sludge	59

Table 1 (*Contd.*)

Analyte(s)	Sample type	Extraction/pretreatment	Analytical technique/ method	Detection limits (LOD/LOQ)	Ref.
6 PFAS: PFBS, PFHxA, PFHpA, PFOA, PFNA, and PFOS	Surface water (Danube river + 14 tributaries); 68 sites across 10 countries; Joint Danube Survey 3 (JDS3), 2013; grab samples (1 L)	SPE (Oasis HLB 200 mg); eluted with ethyl acetate then MeOH + 0.1% NH_3; evaporated; reconstituted in 0.2 mL mobile phase A; $^{13}C/^{18}O$-IS per PFAS; SPM/ fish: ultrasonic extraction (MeOH) + ENVI-Carb cleanup	UHPLC-MS/MS; Waters Acquity + AB SCIEX 5500 QTRAP; ESI negative MRM; BEH C_{18} (50 × 2.1 mm, 1.7 μm); $r^2 \geq 0.986$	LOD: 0.19–1.5 ng L^{-1}; LOQ: 0.55–3.20 ng L^{-1} (analyte-dependent)	60
48 PFAS: PFCAs (PFBA–PFDA), PFSAs (PFBS, PFHxS, PFHpS, PFOS, and PFDS), fluorotelomers (4 : 2 FTSA, 6 : 2 FTSA, and 6 : 2 FTAB, M4) + volatile FTs; plus oxidative conversion for total PFCA precursors	River water + sediment; alluvial groundwater wells (×11); raw and treated water from 3 DWTPs; northern France; 4 campaigns (May–Dec 2013); grab samples	Water (LC-MS/MS): Oasis WAX (200 mg, 6 mL); eluted with MeOH, 0.1% NH_4OH/ MeOH, and 0.1% NH_4OH in iPrOH : DCM (30 : 70); concentrated to 100 μL; water (GC-MS): HS-SPME (DVB/CAR/PDMS 85/50 μm; 50 °C, 30 min; +NaCl); sediment: Freeze-dried; modified Higgins & Luthy extraction	LC-MS/MS: Waters Acquity UPLC + Xevo TQ-MS; ESI negative MRM; BEH C_{18} (2.1 × 50 mm, 1.7 μm); 6 : 2 FTAB/M4: Shimadzu LC + AB SCIEX 5500 QTRAP; GC-MS: Agilent 7890A + ion trap 240 MS; Rxi-624Sil MS (30 m × 0.25 mm, 1.4 μm)	—	61
PFOS and PFOA	Spiked aqueous lab solutions (DI water); batch foam flotation experiments; initial PFOX conc. 20–200 mg L; metallic activators (Al^{3+}, Fe^{3+}, La^{3+}, Ca^{2+}, Fe^{2+}, and K^{+}); pH 2.3–10; Taiwan/USA	No extraction; direct injection of aqueous samples (50 μL) after foam flotation; samples retrieved by syringe from sampling port	HPLC (DIONEX UltiMate 3000) + conductivity detector + anion self-regenerating suppressor (ASRS 300); Acclaim Polar Advantage II C_{18} (150 × 2.1 mm, 3.5 μm); mobile phase: acetonitrile/Milli-Q water/ NaOH–H_3BO_4; flow rate 0.3 mL min^{-1}; gradient mode	LOD: 0.11 mg L^{-1} (PFOS), 0.18 mg L^{-1} (PFOA)	62
26 PFAS: 13 PFCAs (PFBA–PFODA; CF2 3–17), 7 PFSAs (PFBS–PFDS; CF2 4–10), 3 FTS (4 : 2, 6 : 2, and 8 : 2), 3 Cl-PFESAs (C8, C10, and C12)	Tap water, river water (Beijing & Shandong, China) and human urine (highly PFAS-exposed population, Shandong); 10 mL samples; filtered through a 0.7 μm glass-fiber membrane prior to extraction	Fluorous affinity-based DLLME: perfluoro-*tert*-butanol (120 μL, extraction solvent) + acetonitrile (800 μL, dispersive solvent) injected into sample; 3% NaCl (w/v); pH 5 (HCl); equilibrate 5 min; centrifuge 3 min at 4200 rpm; supernatant removed; residue dissolved in 100 μL methanol; 10 μL injected	HPLC-MS/MS: Ultimate 3000 HPLC (ThermoFisher) + API 3200 triple quadrupole (AB SCIEX); ESI negative mode; MRM; Acclaim 120C_{18} (5 μm, 4.6 × 150 mm); mobile phase: MeOH/50 mM NH_4OAc (aq); gradient; flow 1.0 mL min^{-1}	LOD: 0.19–2.6 ng L^{-1} (tap water), 0.18–2.1 ng L^{-1} (river water), 0.28–1.9 ng L^{-1} (urine); LOQ: 0.6–8.7 ng L^{-1} (tap water), 0.6–5.1 ng L^{-1} (river water), 0.9–5.0 ng L^{-1} (urine)	63

Table 1 (*Contd.*)

Analyte(s)	Sample type	Extraction/pretreatment	Analytical technique/ method	Detection limits (LOD/LOQ)	Ref.
6 PFCAs: PFBA, PFPA, PFHA, PFOA, PFNA, and PFDA	Tap, river, wastewater & milk; Xiamen/Zhangzhou, China	MMF-SPME (custom poly(DFHA/VTAC-*co*-DB/ED) monolith, 4-fiber bundle); 20 mL, pH 7.0, 50 min; eluted ACN/TFA (99 : 1); reconstituted in 0.1 mL MeOH; $^{13}C_8$-PFOA IS	HPLC-ESI(−)-MS/MS; Agilent 1290 + Agilent 6400 triple quadrupole mass spectrometer (MS/MS); Kinetex C_{18}; MRM	LOD: 0.40–4.40 ng L^{-1} (water)	64
6 PFAAs: PFHpA, PFOA, PFNA, PFDA (4 PFCAs) + PFHxS, and PFOS (2 PFSAs)	Drinking water (barreled), tap water, pond water, and port water; Jinan, China; filtered (0.45 μm), stored in brown glass bottles at 4 °C	SPE (bamboo charcoal, 300 mg, home-packed cartridge); 100 mL sample, pH 4.0; eluted with 12 mL acetone at 0.5 mL min^{-1}; evaporated under N_2 at 40 °C; reconstituted in 1 mL MeOH	HPLC-ESI(−)-MS/MS; Thermo Ultimate 3000 + AB Sciex QTRAP 5500; Agilent XDB-C_{18} (150 × 2.1 mm, 3.5 μm); 5 mM NH_4Ac/MeOH gradient; 0.4 mL min^{-1}; 40 °C; MRM	LOD: 0.01–1.15 ng L^{-1}; LOQ: 0.03–3.85 ng L^{-1}	65
8 PFCAs: PFHpA, PFOA, PFNA, PFDA, PFUdA, PFDoA, PFTrDA, and PFTeDA	Canal water (industrial discharge, Singapore); 10 mL sample volume	Automated bundled hollow fiber array liquid-phase microextraction (BHF-LPME); dibutyl ether as the extractant; MeOH desorption (200 μL); enrichment factors 9–40	UHPLC-MS/MS (Shimadzu 8060); ESI negative MRM; Zorbax Eclipse plus C_{18} (2.1 × 100 mm, 1.8 μm); mobile phase: 5 mM NH_4COOH in H_2O/5 mM NH_4COOH in MeOH; gradient; 0.3 mL min^{-1}	LOD = 0.40–6.48 ng L^{-1} (except PFDoA: 57.4 ng L^{-1}); LOQ = 1.25–25.6 ng L^{-1} (except PFDoA: 224 ng L^{-1})	66
29 target PFAS: PFBA, PFPeA, PFHxA, PFHpA, PFOA, PFNA, PFDA, PFUnDA, PFDoDA, PFTrDA, PFTeDA, PFBS, PFHxS, PFOS, PFDS, FOSA, 6:2FTSA, 6:2FTUA, 8:2FTUA, 5:3FTCA, and PFOAB (+104 suspect-target PFAS screened; 133 total)	Drinking water — bottled (n = 38) and tap water (n = 59) from 9 countries (Canada, Burkina Faso, Chile, China, France, Ivory Coast, Japan, Mexico, Norway, USA); 1 L sample volume	Automated off-line SPE (Dionex/Thermo Autotrace 280); Strata X-AW cartridges (200 mg/6 mL); conditioned with 0.2% NH_4OH in MeOH + HPLC water; eluted with 2 × 4 mL of 0.2% NH_4OH in MeOH; extract reduced to 400 μL under N_2 at 40 °C	UHPLC–HRMS (Q-Exactive Orbitrap, Thermo); Hypersil Gold C_{18} (100 × 2.1 mm, 1.9 μm); full-scan MS (150–1000 m/z), fast polarity switching; suspect-target screening at ±5 ppm; isotope-labelled IS correction	LOD: 0.010–0.080 ng L^{-1}; LOQ: 0.030–0.23 ng L^{-1}	67
18 PFAS: HFPO-DA, NEtFOSAA, NMeFOSAA, PFBS, PFDA, PFDoA, PFHpA, PFHxS, PFHxA, PFNA, PFOS, PFOA, PFTA, PFTrDA, PFUnA, 11Cl-PF3OUdS, 9Cl-PF3ONS, and ADONA	Drinking water (reagent water and tap water); 250 mL sample volume; preserved with Trizma buffer (5.0 g L^{-1}, pH 7.0)	Manual or automated SPE; SDVB single-polymer cartridges (0.5 g, 6 mL); conditioned with 15 mL MeOH then 18 mL reagent water; sample loaded at 10–15 mL min^{-1}; eluted with MeOH; extract concentrated to dryness under N_2 at ≤65 °C; reconstituted in 1 mL of 96 : 4 MeOH : water; 10 μL injection	LC-ESI(−)-MS/MS (Waters XEVO TQ triple quadrupole); C_{18} column (2.1 × 150 mm, 5 μm); mobile phase: 20 mM NH_4OAc in water/methanol; gradient; 0.3 mL min; negative ESI-MRM; IS correction ($^{13}C_2$-PFOA, $^{13}C_4$-PFOS, d_3-NMeFOSAA)	DL = 0.53–2.8 ng L^{-1}; LCMRL = 0.53–6.3 ng L^{-1}	68

Table 1 (*Contd.*)

Analyte(s)	Sample type	Extraction/pretreatment	Analytical technique/ method	Detection limits (LOD/LOQ)	Ref.
17 PFAS: PFBA, PFPeA, PFHxA, PFHpA, PFOA, PFNA, PFDA, PFUnDA, PFDoDA, PFTeDA, PFHxDA, PFOcDA (12 PFCAs) + PFBS, PFHxS, and PFOS (3 PFSAs) + F-53B + 6 : 2 FTS (14 detected; PFHxDA, PFOcDA, and PFDA not detected in any sample)	Groundwater ($n = 102$) from 550 mL PP bottles, non-industrial well water areas in 13 cities, Jiangsu Province, China (wet season 2016; dry season 2017); also surface water ($n = 12$) and industrial site groundwater ($n = 10$)	SPE (Oasis WAX, 6 cc, 150 mg, Waters); 2 L sample filtered through a 0.45 μm glass fibre membrane; cartridge activated with 4 mL 0.1% NH_4OH/MeOH, 4 mL MeOH, 4 mL Milli-Q water; washed with 4 mL 25 mmol L^{-1} acetate buffer (pH 4); eluted with 4 mL MeOH + 4 mL 0.1% NH_4OH/MeOH; extract concentrated to 1 mL under N_2	HPLC-MS/MS: Shimadzu LC-20AD + AB Sciex API3200 triple quadrupole (ESI^-, MRM); YMC Triart C_{18} column (4.6 × 150 mm, 5 μm) at 40 °C; mobile phase A: 10 mmol L^{-1} NH_4OAc (pH 5)/B: MeOH; gradient 30–90% B over 30 min; flow rate 0.8 mL min^{-1}; injection 10 μL; IS: ^{13}C-labelled surrogates ($^{13}C_4$-PFOS, $^{13}C_4$-PFOA, *etc.*)	LOD = 0.02–0.06 ng L^{-1}; LOQ = 0.08–0.21 ng L^{-1}	69
9 semi-volatile fluorinated compounds: 5 FTOHs (4 : 2 FTOH, 6 : 2 FTOH, 7-Me-6:2 FTOH, 8 : 2 FTOH, and 10 : 2 FTOH) + 2 FOSAs (*N*-MeFOSA and *N*-EtFOSA) + 2 FOSEs (*N*-MeFOSEand *N*-EtFOSE)	River water ($n = 5$) from Llobregat (×2), Ebro (×2) and Fluvià (×1) rivers, Catalonia, Spain; 1000 mL amber glass bottles, stored at 4 °C in dark	SPE (Oasis HLB, 500 mg, 6 mL, Waters); 500 mL sample; conditioned with 20 mL MeOH and 20 mL Milli-Q water; washed with MeOH/water (5 : 95, v/v); eluted with 4 mL MeOH; extract diluted 1 : 3 (v/v) with Milli-Q water	UHPLC-APPI-MS/MS; Accela UHPLC + TSQ Quantum Ultra AM triple quadrupole (Thermo Fisher); Accucore C_{18} (100 × 2.1 mm, 2.6 μm); ACN/ water gradient with 5% toluene post-column dopant; 300 μL min^{-1}; negative-ion APPI-MRM	Instrumental LOD (APPI): 0.08–1 μg L^{-1}; MLOD: 0.3–6 ng L^{-1}; MLOQ: 1–20 ng L^{-1}	70
7 PFCAs (C2–C8): TFA, PFPrA, PFBA, PFPeA, PFHxA, PFHpA, and PFOA	Tap water, groundwater and surface water; Baden-Württemberg, Germany	SPE (Oasis WAX, 150 mg); 50 mL sample pH-adjusted to 3.9; eluted with 0.2% NH_4OH/MeOH through an in-line 0.45 μm filter; reconstituted in H_2O/ MeOH (7 : 3)	LC-ESI(−)-MS/MS; Agilent 1260 + AB Sciex API 5000 triple quadrupole; Kinetex C_{18} (100 × 3 mm, 2.6 μm); NH_4-formate/MeOH gradient; scheduled MRM; isotope-labelled IS	LOD: 0.1–5.5 ng L^{-1}; LOQ: 0.6–26 ng L^{-1}	71
13 PFAS: PFBA, PFPeA, PFHxA, PFHpA, PFOA, PFNA, PFDA, PFUnA, PFDoA, PFTeDA (10 PFCAs) + PFBS, PFHxS, and PFOS (3 PFSAs)	PFAS-contaminated surface water ($n = 6$), Australia; stored in PP falcon tubes at 4 °C	Micro-SPE (ePrep® μSPEed cartridges, 50 : 50 C18 : aminopropyl silica); 2 mL sample, pH 3; eluted with 100 μL 10 mM NaOH/ MeOH; ∼5 min total prep time	UHPLC-ESI(−)-MS/MS; Shimadzu Nexera MP + LCMS-8060 triple quadrupole; Luna Omega C_{18} (50 × 2.1 mm, 1.6 μm); H_2O/MeOH gradient; MRM; ^{13}C-IS	LOD: 0.29–6.6 ng L^{-1}	72
PFOA	Tap water, rainwater, and seawater; Sydney, NSW, Australia; stored at 4 °C	MOF-SPME (ZIF-8-coated stainless-steel needle, poly(dopamine) adhesion layer); 5 mL sample, 3 min immersion; desorbed into ∼10 μL MeOH; no sample prep required; ∼5 min total	nESI-MS; Thermo LTQ XL linear ion trap; negative ion mode; direct infusion; PFHxA as IS; standard addition for seawater	LOD: 11.0 ng L^{-1}	73

PFBS, and PFOA with good precision over 5 days.[49] Further innovations include large-volume-injection HPLC combined with micro liquid–liquid extraction (μ-LLE), enabling identification of previously undetected PFAS in groundwater with method LODs of 0.71–67 ng L^{-1};[50] when supplemented with filtration and centrifugation, QTOF-MS extended this further, facilitating identification of up to 40 novel PFAS classes in AFFF-impacted groundwater.[51]

Over the past two decades, liquid chromatography coupled with electrospray-ionisation tandem mass spectrometry (LC-ESI-MS/MS) has become a reliable approach for the precise and reproducible quantification of PFAS, particularly for long-chain legacy compounds. For instance, Li *et al.* applied UPLC/ESI-MS/MS to identify PFAS in lake sediments after ultrasonication extraction in methanol, reporting total PFAS concentrations of 0.61–26 ng g^{-1} with spike recoveries (88–102%) and minimal matrix interference.[52]

Taken together, these chromatographic and high-resolution mass-spectrometric approaches offer robust coverage across PFAS classes while highlighting a practical constraint: they remain resource-intensive, require maintenance in centralised facilities and are not easily deployed *in situ*. Despite this level of performance by coupled chromatographic techniques, trace-level occurrence of PFAS, significant matrix interferences, and their dependence on pre-treatment steps (such as SPE and liquid–liquid extraction),[33] complicate the quantification. Their limited portability and high operating costs further constrain real-time and *in situ* monitoring. This gap is a key motivation for the development of rapid platforms discussed in the subsequent sections.

Table 1 summarises chromatographic methods for PFAS detection in water samples with parameters such as analytes, sample type, extraction/pretreatment methods, techniques and detection limits.

The following sections examine PFAS detection platforms for sensor-based detection (Sections 3 and 4) and separation-coupled based (Section 5) approaches. Optical and electrochemical sensors transduce a molecular recognition event directly into a measurable signal without requiring prior analyte separation. Electrophoresis, on the other hand, first resolves PFAS compounds based on charge-to-size ratios before quantification *via* a coupled detector. Together, these approaches span a broad spectrum from high-resolution laboratory separation to rapid field-deployable sensing.

3. Optical sensor-based detection

The working principle of optical sensors primarily involves the detection of changes in light intensity and the subsequent conversion of these variations into measurable electrical signals.[74] An optical sensor generally comprises two main elements: a transducer and a recognition unit. The various changes in the optical properties of the transducer surface, on interaction with target analytes within complex environmental matrices govern the overall performance of the sensor. These systems offer excellent sensitivity, chemical stability, and straightforward signal interpretation. However, their dependence on the careful selection of light wavelengths to ensure reliable sensing and imaging applications remains a key limitation. Several optical techniques have been investigated for PFAS detection, including optical fibres, and colorimetric and fluorescence-based methods, owing to their high sensitivity and suitability for environmental monitoring.[75]

3.1. Optical fibre sensors (OFS)

OFS are broadly categorized as intrinsic or extrinsic, depending on the manner in which the optical field interacts with the target analyte. In intrinsic sensor configurations, the optical fibre itself constitutes an integral part of the sensing region, where variations in temperature, refractive index, strain, or chemical composition of the surrounding environment directly modulate the properties of the light propagating through the fibre, including intensity, phase, wavelength, or polarization.[76] By contrast, extrinsic OFS utilise the fibre primarily as a light-guiding medium, transmitting optical signals to and from an external sensing element where interactions with the analyte take place. This distinction enables flexible sensor design tailored to specific analytical requirements. Due to their structural versatility and compatibility with diverse transduction mechanisms, OFS have found widespread application across environmental monitoring, biomedical diagnostics, chemical process control, and industrial safety systems. Their principal advantages include relatively low fabrication and maintenance costs, capability for real-time and remote operation, immunity to electromagnetic interference, mechanical robustness under harsh environmental conditions, and straightforward surface functionalization for selective analyte recognition.[77] These attributes make them especially suitable for deployment in distributed sensing networks and *in situ* monitoring scenarios.

Among the available waveguiding materials, plastic optical fibres (POFs) are particularly attractive for sensing applications because of their mechanical flexibility, ease of handling and machining, and comparatively large core diameter, which facilitates efficient light coupling and improves signal stability.[78] POFs also exhibit higher fracture toughness than silica fibres, making them advantageous in portable, wearable, or field-deployed sensing platforms where mechanical resilience is essential. Furthermore, optical fibre sensing systems can be integrated into distributed architectures and satellite-linked communication networks, enabling remote and large-scale environmental surveillance.[79] Such integration bridges the gap between highly sensitive laboratory-based analytical techniques and practical, field-deployable monitoring solutions, thereby supporting continuous and geographically extensive data acquisition. A diverse range of optical fibre-based sensing platforms has been developed for PFAS detection. These include evanescent-field sensors, surface plasmon resonance (SPR)-based configurations, and interferometric designs, each offering distinct advantages in sensitivity and selectivity. To enhance molecular recognition, these platforms are commonly functionalized with selective layers such as molecularly imprinted polymers (MIPs), monoclonal antibodies, and fluorinated absorptive coatings, enabling improved affinity, specificity, and detection performance in complex environmental matrices. A D-shaped POF substrate, incorporating

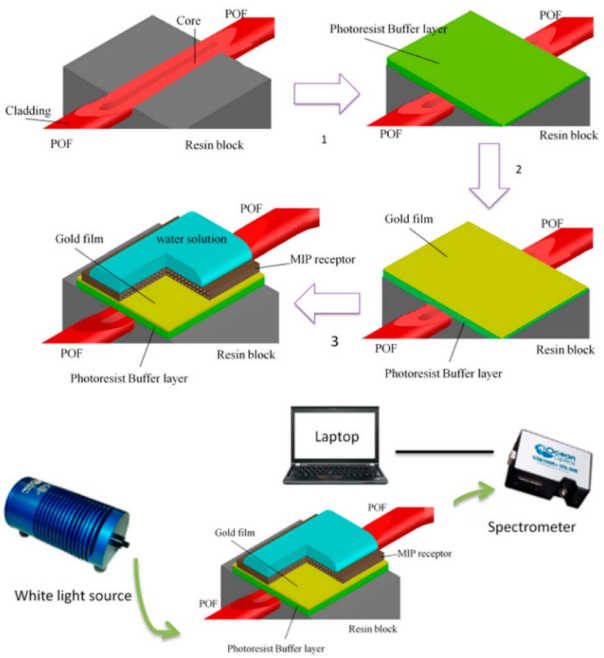

Fig. 2 Production steps for realizing an SPR sensor in a D-shaped POF with an MIP receptor and outline of the experimental setup.[80] Reproduced from ref. 80 © 2018 by the authors. Licensee MDPI, Basel, Switzerland. This article is an open access article distributed under the terms and conditions of the Creative Commons Attribution (CC BY) license (http://creativecommons.org/licenses/by/4.0/).

a photoresist buffer layer and a 60 nm sputtered gold film monitored by a compact halogen-lamp spectrometer was reported.[80] Replacing the antibody receptor with a MIP achieved a comparable LOD of 0.13 μg L^{-1} *vs.* 0.24 μg L^{-1} for the antibody-based sensor, across a detection range of 0–4 μg L^{-1} for PFOA. The key advantage of the MIP over the antibody lies in its greater stability, reproducibility, and lower cost rather than a significant gain in sensitivity. This was achieved with a blue shift in resonance wavelength confirming a reduction in the effective refractive index of the MIP layer upon PFAS binding (Fig. 2).[80]

In a cost-efficient design, a polished D-shaped plastic optical fibre coated with an ammonium perfluorooctanoate-templated MIP and read using a single LED and dual photodiodes produced a self-referenced intensity signal after approximately 10 minutes of incubation. This achieved a LOD of 0.5 μg L^{-1} and a working range of 0.5–200 μg L^{-1} for PFOA (with the MIP designed for broad C4–C12 PFAs recognition).[81] A complementary bio-recognition system immobilised a monoclonal antibody specific to PFOA and PFOS on the gold surface through an α-lipoic acid self-assembled monolayer and EDC/NHS coupling. Using an SPR-based plastic optical fibre immunosensor, Cennamo *et al.* (2018) reported a LOD of 0.21 μg L^{-1} within a range of 0–100 μg L^{-1} for PFOA and PFOS, with selectivity retained in matrices mimicking real environmental conditions.[82] For shorter-chain compounds, an SPR-based plastic optical fibre (SPR-POF) tailored to PFBS and integrated with a compact LED/Arduino setup demonstrated low sensitivity, aligning well with portable, minute-scale field analysis.[83] For higher-concentration screening, a cleaved silica-fibre Fabry–Pérot device coated with a thin PVDF film achieved a LOD of ~5 ppm and a working range of 5–60 ppm for PFOA, showing responses in aqueous film-forming foam (AFFF)-impacted samples (Fig. 3).[84]

Temperature sensitivity and stabilisation time remain key engineering challenges before field deployment.[84] Collectively, these studies demonstrate that both recognition chemistry and transduction design determine the balance between sub-ppb sensitivity and practical field operation. These studies also highlight future priorities such as improving selectivity in complex matrices, developing antifouling surfaces, miniaturising hardware, and integrating automated or networked readout systems for scalable environmental monitoring.

Table 2 summarises representative examples (optical fibre sensors), including performance parameters and associated references.[80–84]

3.2. Colorimetric sensors

A widely explored analytical approach for PFAS detection is colorimetric sensing, which is valued for its rapid response, affordability, and ease of use. This technique relies on detecting

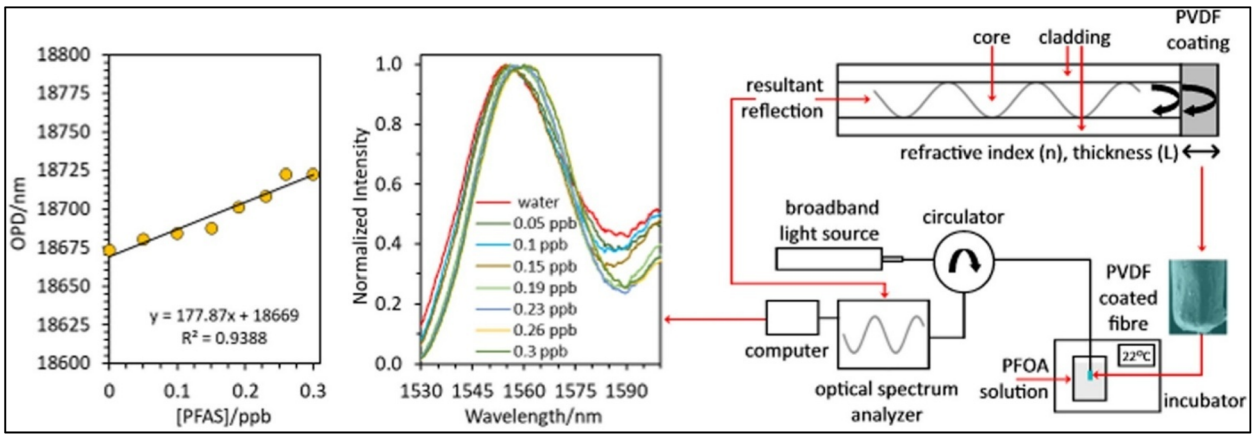

Fig. 3 Graphical abstract: polyvinylidene fluoride coated optical fibre for detecting perfluorinated chemicals.[84] Reproduced from ref. 84 Copyright (2020) with permission from Elsevier.

Table 2 Overview of optical fibre sensors for PFAS detection

Analyte(s)	Description/title	Recognition/receptor & fibre/transducer	Read-out setup	LOD	Ref.
PFOA	A molecularly imprinted polymer on a plasmonic plastic optical fiber to detect perfluorinated compounds in water	SPR-POF-MIP sensor: a molecularly imprinted polymer (MIP) combined with a surface plasmon resonance (SPR) plastic optical fiber (POF) platform. A D-shaped plastic optical fiber (POF) covered with a photoresist buffer layer and a thin gold film (60 nm) MIP: the prepolymeric mixture for the MIP was prepared based on ammonium perfluorooctanoate (FPO–NH_4) as the template, VBT and PFDA as the functional monomers, EDMA as the cross-linker and AIBN as the radicalic initiator	Halogen lamp (HL-2000-LL) and a spectrometer (FLAME-S-VIS-NIR-ES) (SPR wavelength shift)	0.13 ppb	80
PFOA	A simple and low-cost optical fiber intensity-based configuration for perfluorinated compounds in water solution	MIP receptor deposited on a simple D-shaped POF platform. Characterized using a setup based on an LED and two photodetectors. D-Shaped POF & intensity-based (evanescent field) configuration MIP: the pre-polymeric mixture of the MIP was prepared using ammonium perfluorooctanoate (FPO–NH_4) as the template, VBT and PFDA as the functional monomers, EDMA as the cross-linker and AIBN as the radicalic initiator	Experimental setup based on an LED (627 nm), an optical coupler (50 : 50), two photodetectors, and digital oscilloscope (Picoscope) connected to laptop	0.5 ppb	81
PFOA/PFOS	A high sensitivity biosensor to detect the presence of perfluorinated compounds in environment	SPR optical fiber biosensor system: the optical sensor platform is based on surface plasmon resonance (SPR) in a D-shaped POF, with a photoresist buffer layer (1.5 μm) between the exposed POF core and the thin gold film (60 nm); SPR transducer Immobilization process: the surface of the chip was pre-treated before the covalent immobilization of mono specific antibody and the procedure consists: (1) thiol film production, (2) derivatization by EDC/NHS and (3) antibody against PFOA/PFOS immobilization	Halogen lamp (HL-2000-LL) & spectrometer (FLAME-S-VIS-NIR-ES) (SPR wavelength shift)	<0.21 ppb	82
PFBS	Water monitoring in smart cities exploiting plastic optical fibers and molecularly imprinted polymers. The case of PFBS detection	SPR-POF-MIP sensor: D-shaped POF with a photoresist S1813 layer (an optical buffer layer) and a thin gold film (60 nm thick); SPR transducer MIP: the prepolymeric mixture for the MIP was prepared based on ammonium perfluorooctanoate (FPO–NH_4) as the template, VBT and PFDA as the functional monomers, EDMA as the cross-linker and AIBN as the radicalic initiator	White light source (HL-2000-LL) & a spectrometer (USB2000 + UV-VIS-ES), connected to a Raspberry Pi (Pi 2)	<1 ppb	83
PFOA (model); PFAS mixture (AFFF)	Polyvinylidene fluoride coated optical fibre for detecting perfluorinated chemicals	A Fabry-Perot Interferometry (FPI) based optical fibre to detect PFOA/PFAS in aqueous solutions. The fabrication procedure utilized an immersion precipitation-based phase inversion process to form a thin polyvinylidene fluoride (PVDF) coating at the end-faces of freshly cleaved optical fibres. PVDF coating was rich in the electroactive β-phase and enhances dipole–dipole & hydrophobic interactions at binding sites	ANDO AQ6317B optical spectrum Analyzer (OSA), Erbium Broadband Source (EBS) and a three-port optical circulator	~5 ppm (PFOA)	84

changes in colour intensity when PFAS interact with specific reagents, allowing for simple optical measurement.[85] However, despite its advantages, colorimetric sensing is often limited by lower precision compared to other analytical methods.[86] Several attempts focus on strategies to enhance the analytical sensitivity of colorimetric practices and methods.

Colorimetric detection usually relies on optical responses resulting from chemical and physicochemical interactions between PFAS compounds and responsive molecules, dyes, polymers, and even nanoparticles. The responsive molecules change their optical properties (absorbance, wavelength, and even colour transitions), which are usually detected using spectrophotometers. The detection of PFAS using the colorimetric method is desirable because of the possibility of using less expensive detection tools. However, more research is still needed to improve the required selectivity and sensitivity.

Nanoparticle-assisted colorimetric assays typically combine a signal-enhancing nanomaterial with a chromogenic dye, producing a measurable spectral response upon PFAS interaction that can be recorded using simple optical setups or smartphone-based readers.[13,87] Silver and gold nanoparticles are the most widely employed nanomaterials in this context owing to their strong localised surface plasmon resonance (LSPR) properties, which amplify optical signal intensity. Upon PFAS-induced aggregation, inter-particle LSPR coupling generates a bathochromic band shift, a visible red-to-blue/purple colour change in the extinction spectrum, serving as the primary colorimetric readout.[87] Iron oxide nanoparticles, by contrast, act as peroxidase-mimic nanozymes, catalysing the oxidation of 3,3′,5,5′-tetramethylbenzidine (TMB) to its oxidised form (oxTMB). When magnetic in nature (*e.g.* Fe_3O_4), these particles additionally enable rapid magnetic separation and sample preconcentration, simplifying matrix handling prior to the colorimetric readout step.[13,87] Colour development in these systems therefore arises through one of two distinct mechanisms: direct chromophoric absorption of the dye–PFAS ion-pair complex, or LSPR-mediated bathochromic shifts driven by nanoparticle aggregation. The primary driving force governing PFAS–dye association is electrostatic attraction between anionic PFAS headgroups, sulfonate or carboxylate, and cationic chromophores such as methylene blue or ethyl violet, with hydrophobic and fluorous interactions along the perfluorocarbon chain providing additional stabilisation of the complex.[13,87]

The majority of dye-based colorimetric reports have focused on anionic PFAS, particularly PFOS and PFOA, which are the most tractable targets for cationic dye-based detection given their well-defined anionic headgroups.[13,87] In methylene blue-based assays, PFAS binding produces a hypsochromic shift in the characteristic absorption band at ~664 nm, with the magnitude of the shift correlating linearly with PFAS concentration over a reported range of 0.1–2 mg L^{-1}. In nanozyme-based platforms, PFOS groups adsorb onto Fe_3O_4 surfaces *via* electrostatic and hydrogen-bonding interactions, inhibiting TMB oxidation and producing a concentration-dependent decrease in absorbance at 652 nm.[87] In contrast, colorimetric detection of cationic PFAS (*e.g.*, fluorinated quaternary ammonium surfactants) and zwitterionic PFAS remains largely undeveloped, as these charge classes do not interact favourably with the cationic dyes employed in conventional assays and require receptor systems capable of simultaneously accommodating structurally distinct charge arrangements – a substantially more complex design challenge that is yet to be systematically addressed.[13,87]

The selectivity of colorimetric PFAS sensors is principally governed by the thermodynamics of dye–PFAS ion-pair formation, with the fluorocarbon chain length playing a critical modulating role. Experimental data from both AuNP aggregation-based and nanozyme inhibition assays consistently show that short-chain PFAS ($C < 7$) produce substantially reduced signal responses relative to long-chain homologues under equivalent concentration conditions. This finding is attributed to their lower hydrophobicity and correspondingly weaker fluorous stabilisation of the ion pair.[87] This chain-length dependence of binding affinity creates a competitive binding problem in environmental samples: long-chain PFAS compete with short-chain homologues (*e.g.*, PFBS and PFBA) and with non-target anionic surfactants such as sodium dodecyl sulfate (SDS) and sodium dodecylbenzenesulfonate (SDBS) which bear analogous sulfonate functional groups, for the same cationic dye binding sites, potentially causing signal overestimation.[13] Additionally, matrix constituents common in real water samples, particularly dissolved organic matter (DOM), humic acids, and divalent cations (Ca^{2+} and Mg^{2+}), can independently induce nanoparticle aggregation or competitively displace PFAS from dye-binding sites, generating false-positive colorimetric responses.[77] Two principal strategies have been reported to address these interferences. First, fluoro-SPE preconcentration selectively retains fluorinated surfactants on a fluorinated gel while washing through non-fluorinated co-contaminants; when combined with an upstream SDVB-SPE step, this approach achieves an LOD of 1 ppb for PFOA, PFOS, and 6 : 2 FTS in spiked tap and groundwater.[88] Second, pH adjustment to circumneutral conditions is routinely applied to maximise ion-pair stability between the dye and PFAS headgroup. Mahpishanian *et al.* demonstrated the optimal performance at pH 7.1 in phosphate buffer.[89]

Despite these advances, the sensitivity of colorimetric PFAS platforms varies considerably with detection architecture. Simple aggregation-based assays using functionalised AuNPs yield LODs in the range of 10–100 μg L^{-1}, constrained by relatively modest signal amplification, while peroxidase-mimic nanozyme platforms such as MoS_2–Fe_3O_4 nanocomposites improve this to approximately 4.3 μg L^{-1} for PFOS.[87] Advanced oxidase-mimic systems based on cobalt-embedded nitrogen-doped carbon nanosheets (CoNCN) have achieved LODs as low as 0.02 μg L^{-1}, among the lowest reported for dye-based colorimetric detection, though such performance reflects optimised laboratory conditions and does not represent field-deployable sensitivity.[87] Portable, smartphone-based implementations such as the astkCARE kit, which employs ethyl violet and ethyl acetate extraction, report an LOD of ~10 ppb without preconcentration, reducible to ~0.5 ppb following SPE, and produce semi-quantitative results within tens of

minutes.[88,90] By comparison, fibre-optic SPR sensors employing a plastic optical fibre (POF) with a MIP receptor achieve a detection limit of 0.13 μg L^{-1},[80] while the US EPA drinking water method reported by Shoemaker *et al.*, using solid-phase extraction coupled with LC-MS/MS, demonstrates analyte-specific detection limits of 0.5–6.5 ng L^{-1} across 14 per-fluoroalkyl acids (PFAAs), with minimum reporting levels of 2.9–14 ng L^{-1}.[29] Since PFAS occur in environmental waters at concentrations spanning the sub-ppt to low-ppb range,[13] most colorimetric platforms require sample preconcentration (*via* SDVB-SPE, fluoro-SPE, or liquid–liquid extraction) to approach the detection thresholds required by regulatory frameworks.[88]

Liu *et al.* synthesised MoS_2–Fe_3O_4 nanocomposites through a solvothermal process for PFOS quantification.[91] These nanocomposites exhibited intrinsic peroxidase-like activity, enabling catalytic oxidation of chromogenic substrate TMB, leading to the formation of a distinct blue coloration. The presence of sulfonate groups in solution facilitated PFOS binding to the MoS_2–Fe_3O_4 surface *via* electrostatic interactions, thereby inhibiting the catalytic reaction and altering the colorimetric response. Fig. 4A provides a schematic illustration of the colorimetric sensing mechanism, highlighting how the MoS_2–Fe_3O_4 nanocomposite catalyses the oxidation of TMB in the presence of hydrogen peroxide (H_2O_2) to generate a blue-coloured product (oxTMB). When PFOS is introduced, the interaction with the nanocomposite reduces peroxidase activity, resulting in a diminished colour intensity. Fig. 4B presents the corresponding absorbance spectra recorded in the presence and absence of PFOS, validating the sensing response. Fig. 4B(a) demonstrates the increase in the TMB oxidation signal upon addition of the MoS_2–Fe_3O_4 nanocomposite, while Fig. 4B(b) shows the concentration-dependent absorbance enhancement with increasing nanocomposite loading. Fig. 4B(c) compares the absorbance under different reaction conditions in the presence of PFOS, with the inset showing visible colour changes across Fe_3O_4, MoS_2, MoS_2 + Fe_3O_4, and MoS_2/Fe_3O_4 systems.[91] This sensing strategy reported a linear detection range from 0.1 to 12.5 μM, with an LOD of 8.6 nM. Given their robust catalytic activity, ease of synthesis, and low-cost fabrication, the MoS_2/Fe_3O_4 nanocomposite seems to be a promising platform for biosensing and catalytic applications. Their adaptability allows for potential expansion into novel PFAS detection techniques utilising diverse sensing mechanisms.[91]

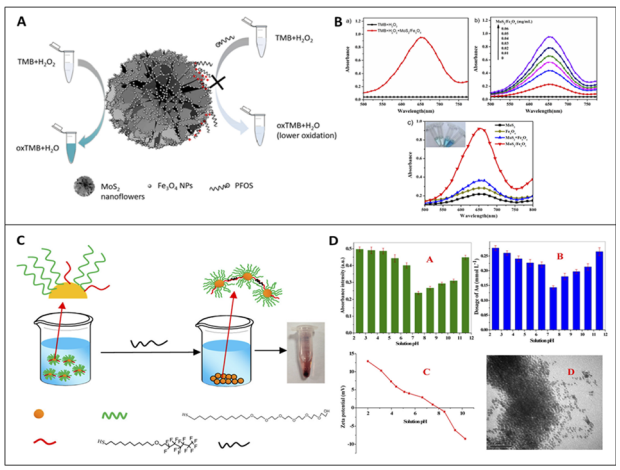

Fig. 4 (A) Schematic illustration of colorimetric sensing detection of PFOS. (B) Absorbance curves of (a) the colorimetric system containing a TMB substrate with or without our-prepared nanocomposites, (b) different concentrations of MoS_2/Fe_3O_4 nanocomposites, (c) different reaction systems. Inset images of color changes (from left to right corresponding to Fe_3O_4, MoS_2, MoS_2 + Fe_3O_4, MoS_2/Fe_3O_4).[91] Reproduced from ref. 91 Copyright (2019) with permission from Elsevier. (C) Mechanistic assay for colorimetric detection of PFCs with perfluorinated and PEG thiols modified Au NPs. (D) Absorbance (A), concentration of the Au element (B), and ζ-potential (C) of Au@PEG-F NPs suspension at different pHs, and TEM image of Au@PEG-F NPs (D) at pH 7.5.[92] Reproduced from ref. 92 Copyright (2014) with permission from American Chemical Society.

Niu *et al.* (2014) introduced a sensing approach for the colorimetric detection of PFCs, which is illustrated in Fig. 4C.[92] This mechanism relies on fluorous–fluorous interactions, where gold nanoparticles (Au@PEG-F NPs) are functionalised with a combination of poly(ethylene glycol)-terminated (PEG-thiols) and perfluoroalkyl-terminated (F-thiols) thiols to enhance specificity. The structural changes induced by PFC binding result in a visible colour shift, allowing for detection. The quantitative analysis presented in Fig. 4D further validates the performance of the Au@PEG-F NPs under different pH conditions.[92] Graphs (Fig. 4D(A) and (B)) indicate how pH influences the absorbance and Au element concentration, reflecting the stability of the modified nanoparticles. The zeta (ζ)-potential measurements in Fig. 4D(C) provide insights into surface charge variations, demonstrating nanoparticle stability across the pH spectrum. Additionally, the TEM image in Fig. 4D(D) depicts the morphology of the nanoparticles at pH 7.5, showcasing their well-dispersed nature. This method reported a detection range between 0.1 and 1000 μg L^{-1} and an LOD of 10 μg L^{-1}. Given its sensitivity and stability aspects, the authors reported this as a promising approach for monitoring total PFC concentrations in water samples.[92]

Fang *et al.* (2018) reported a smartphone-based analytical tool designed for detecting anionic surfactants, including PFOA and PFOS.[93] The detection approach is analogous to the methylene blue active substances (MBAS) method, employing liquid-phase extraction (LPE) to transfer the hydrophobic ion-pair complex formed between ethyl violet dye and the anionic surfactant into an organic solvent (ethyl acetate). The colour (RGB) of the organic phase is then captured using a smartphone camera within a specialised reading kit, and the RGB values are calibrated and correlated with anionic surfactant concentration, maintaining a standard deviation below 10% across the 10–1000 ppb range. The system's design and functionality are illustrated across the six panels of Fig. 5. Fig. 5a shows the app's calibration function interface alongside integrated online help features, enabling operation by non-specialist users in the field. Fig. 5b depicts the reading screen, where the measurement zone is precisely positioned over the non-aqueous phase layer, with the inner square defining the colour-reading area for RGB analysis. Fig. 5c summarises a completed measurement output, displaying a result of 390 ppb, with GPS location logging and

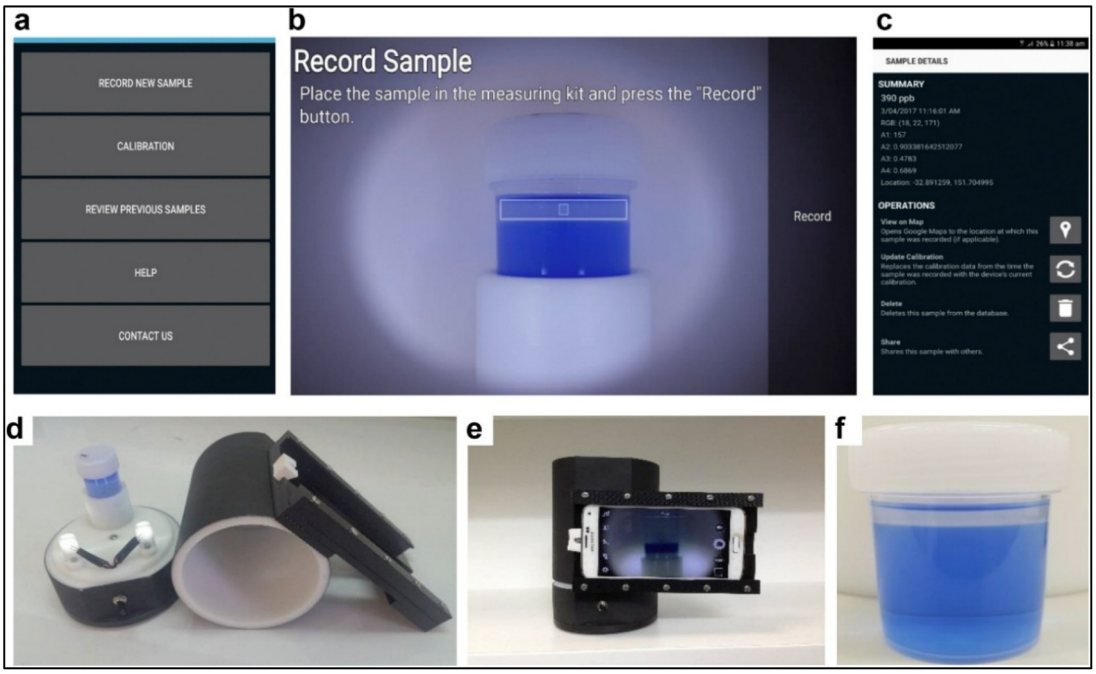

Fig. 5 Snapshots (a–c) of the app, photos of reading kit (d and e) and sample (b and f). In (b), the reading screen's rectangle zone is positioned over the non-aqueous phase layer and the central part (inner square) is the colour reading area. In (d), two white LEDs are on and a container of 25 mL containing the sample is positioned in a sample holder. In (e), the smartphone holder is shown holding a smartphone in the reading position. Note the smartphone's different rotated orientation (portrait or landscape) in (a–c and e).[93] Reproduced from ref. 93 Copyright (2018) with permission from Elsevier.

options to share data *via* Bluetooth or email, key features for field deployment and remote reporting. Fig. 5d shows the sample holder equipped with two white LEDs, which provide consistent background illumination to eliminate variability under ambient lighting conditions. Fig. 5e shows the adjustable smartphone holder securing the device within the reading kit at a fixed distance and angle for stable, reproducible image capture. Fig. 5f shows the polypropylene sample container, with the extracted organic phase visible as the top layer, the central portion of which serves as the colour-reading area. The system detects PFOA in tap and groundwater with an LOD of 10 ppb (~24 nM) using a dual-LPE method in approximately 5 minutes. Integrating a more sensitive solid-phase extraction pre-concentration step further lowers the LOD to 0.5 ppb (~1.21 nM), albeit over a longer processing time of approximately 3 hours. This portable tool demonstrates potential for both field applications and routine laboratory pre-screening, offering a rapid and cost-effective alternative to centralised LC-MS analysis for on-site environmental monitoring.[93]

Fluoro-solid phase extraction (fluoro-SPE) has been well established to selectively extract targets after they have been fluoro-tagged. Al Amin *et al.* reported extraction using the astkCARE reagent to form an anionic surfactant-cationic dye ion-pair, which is similar to MBAS.[88] This ion-pair is immiscible in aqueous solution and therefore can be extracted to the organic phase for colour justification. Based on the colour, a visual assessment or smartphone-based app can relate it to the concentration level.[88] In order to improve the sensitivity, styrene-divinylbenzene solid-phase extraction (SDVB-SPE) was employed to concentrate the sample from 500 mL to 5 mL, and simultaneously, fluoro-SPE was employed to selectively isolate fluorinated surfactants (FS) from other anionic surfactants. This approach seems highly effective, reporting an LOD as low as 1 ppb for PFOA, PFOS and fluorotelomer sulfonate. The results confirm that FS detection can be successfully conducted in conventional laboratory settings equipped with standard extraction techniques, making this method a practical and reliable tool for environmental monitoring.

Table 3 summarises colorimetric PFAS sensors, detailing the key parameters and detection limits.

3.3. Fluorescent sensors

Fluorescent detection relies on fluorescence resonance energy transfer (FRET), a non-radiative energy transfer mechanism in which an excited-state donor dye transfers energy to an acceptor molecule, such as silver or gold nanoparticles (NPs), *via* dipole–dipole interactions. This process plays a crucial role in sensor technologies, particularly for detecting PFAS, as it enables sensitive and selective fluorescence-based measurements.[96] The effectiveness of FRET-based sensing lies in its ability to modulate fluorescence intensity in response to molecular interactions. In fluorescence-based PFAS sensors, the binding event between PFAS and the fluorescent probe or receptor is characterised by a dissociation constant (K_D) that reflects the thermodynamic affinity of the interaction. For aptamer-based fluorescent sensors targeting PFOA, reported K_D values are in

Table 3 Colorimetric sensors for PFAS analysis in various water samples

Analyte(s)	Sample type	Description/title	Probe/detection approach	LOD	Ref.
PFOA, PFOS, 6 : 2 FTS	Aqueous PFAS solutions (extracts after SPE and fluoro-SPE)	Smartphone-based/Fluoro-SPE for selective detection of PFAS at ppb level	Smartphone-based colorimetric detection coupled with SPE (pre-concentration) and fluoro-SPE (pre-selection). Ethyl violet dye with SDVB-SPE preconcentration and fluoro-gel fluoro-SPE	1 ppb	88
PFOS	Aqueous PFOS solutions	A facile solvothermal synthesis of 3D magnetic MoS_2/Fe_3O_4 nanocomposites with enhanced peroxidase-mimicking activity and colorimetric detection of perfluorooctane sulfonate	MoS_2/Fe_3O_4 nanocomposite accompanied by peroxidase-mimicking catalytic activities enhancement through a facile solvothermal method. Colorimetric reaction involves TMB & H_2O_2. Absorbance changes at 652 nm recorded	8.6 nM	91
Perfluorinated compounds (PFCs, perfluoroalkyl chain ≥7)	Tap water & river water	Sensitive colorimetric visualization of perfluorinated compounds using poly(ethylene glycol) and perfluorinated thiols modified gold nanoparticles	AuNP based colorimetric assay (aggregation). Sensing probe: mixed poly(ethylene glycol)-terminated (PEG-thiols) and perfluoroalkyl-terminated (F-thiols) alkanethiols modified gold nanoparticles (Au@PEG-F NPs)	PFCs: as low as 10 ppb	92
PFOA/PFOS	Milli-Q water, tap water, and groundwater (after SPE or dual-LPE treatment)	Smartphone app-based/portable sensor for the detection of fluoro-surfactant PFOA	Smartphone app-based colorimetric assay for anionic surfactants (AS) detection. Liquid-phase extraction (LPE) is employed to extract the hydrophobic ion-pair of dye (ethyl violet)-AS to an organic phase (ethyl acetate); smartphone RGB readout	10 ppb	93
PFOS	Water samples (tap & river)	A new dual-recognition strategy for hybrid ratiometric and ratiometric sensing perfluorooctane sulfonic acid based on high fluorescent carbon dots with ethidium bromide	A hybrid ratiometric nanosensor was designed *via* two recognition strategies: (i) simultaneous application of fluorescence & light scattering and (ii) dual-color ratiometric sensing by linking blue-green-emitting nitrogen-doped carbon dots with orange-red-emitting ethidium bromide (N-CDs/EB). To achieve colorimetric detection, with the help of EB, the fluorescence of the system changed from green to orange	27.8 nM	94
PFOS	Environmental water samples (lake & river)	A resonance Rayleigh scattering and colorimetric dual-channel sensor for sensitive detection of perfluorooctane sulfonate based on toluidine blue	Resonance Rayleigh scattering (RRS) and colorimetric dual-channel sensor based on toluidine blue (TB) for PFOS detection	4.2 nmol L^{-1} (RRS) & 112 nmol L^{-1} (colorimetry)	95

the low micromolar range (~5.5 μM), indicating moderate binding affinity that is sensitive to the length of the fluorinated carbon chain rather than the terminal functional group. Structurally similar PFAS analogues (*e.g.*, PFHpA and PFHxS) exhibit comparable K_D values (3.3–6.5 μM), meaning that competitive binding from non-target congeners present in real samples can attenuate or amplify the fluorescence signal in a concentration-dependent manner, complicating quantification.[97,98]

Fluorescent sensors are typically categorised as "turn-on" or "turn-off" systems, where fluorescence is either enhanced or quenched upon PFAS binding. Fluorescence "turn-on" sensing strategies operate by enhancing emission intensity upon interaction with the target analyte, thereby improving sensitivity and facilitating detection in complex environmental matrices. On the other hand, in the "turn-off" mechanism, the intensity of fluorescence decreases following PFAS interactions due to complex formation or quenching effects, thereby allowing sensitive and selective PFAS detection with detection limits ranging from ng L^{-1} to μg L^{-1}. The direct interaction between the fluorescent probe and the target analytes leads to detectable shifts in fluorescence emission. The extent of this change correlates with the analyte concentration, making FRET-based fluorescence sensing a valuable tool for quantitative PFAS detection.[99]

For systems relying on electrostatic quenching or FRET mechanisms (*e.g.*, CDs–berberine and HPTS–chitosan), co-existing anions (phosphate, chloride, and nitrate) in real water samples can competitively interact with the positively charged receptor surface, suppressing PFAS-induced fluorescence recovery and shifting apparent detection thresholds. Matrix effects from natural organic matter can also directly quench fluorophore emission through the inner filter effect (IFE), introducing concentration-dependent errors in complex water samples.[77,100] Studies applying these sensors to environmental water samples typically report increased relative standard deviation (RSD) and reduced recoveries compared to pure aqueous calibration standards, underscoring the need for matrix-matched calibration or standard addition methods for accurate field quantification.

Liu *et al.* (2015) reported a fluorescence-based sensing approach utilising 3-mercaptopropionic acid (MPA)-cadmium sulfide (CdS) quantum dots (QDs) that is both rapid and sensitive for detecting PFOA.[101] Through characterisation techniques such as TEM, FTIR, zeta potential analysis, and fluorescence spectroscopy, they established that PFOA interacts with the surface of MPA-CdS QDs, leading to considerable nanoparticle aggregation. This interaction subsequently results in fluorescence quenching. The proposed method enables PFOA detection within roughly 10 minutes, offering a detection range of 0.5 to 40 μM and an LOD of 0.3 μM. Their findings highlight a strategy for designing nanoparticle-based fluorescent assays for PFOA analysis.[101]

Chen *et al.* (2019) developed a highly efficient triple-channel optical assay for PFOS detection, utilising carbon quantum dots (CDs) synthesised through a one-pot hydrothermal method.[102] These CDs served as a sensing probe, interacting with PFOS to form a ground-state complex, which in turn altered fluorescence intensity, UV-vis absorption, and resonance light scattering (RLS) signals. The method reported an LOD of 18.27 nM for PFOS. Moreover, this approach was validated for PFOS detection in real water samples, maintaining a RSD of ≤2.09%. This advancement further broadens the scope of nanoparticle-based fluorescent assays for detecting perfluorinated compounds in environmental samples (Fig. 6a).[102] Building on this progress, Chen *et al.* (2020) introduced a straightforward hybrid ratiometric nanosensor for PFOS detection, integrating two distinct recognition strategies.[94] The first approach utilised both fluorescence and light scattering techniques, while the second involved the development of a dual-colour ratiometric sensor by coupling blue-green-emitting nitrogen-doped carbon dots with orange-red-emitting ethidium bromide. This nanosensor exhibited a strong linear correlation with PFOS concentrations in the range of 0–2.0 μM, and exhibited an LOD of 27.8 nM, making it suitable for detecting PFOS in aqueous environments. These findings suggest that this ratiometric nanosensor holds promise for environmental monitoring applications, further expanding the capabilities of nanoparticle-based detection strategies for perfluorinated pollutants.[94]

Cheng *et al.* (2018) reported a fluorescence enhancement method for PFOA and PFOS based on the interaction between erythrosine B (EB) and hexadecyltrimethylammonium bromide (CTAB).[106] Under mildly basic conditions (pH 8.5), EB formed a fluorescent complex with CTAB, and the addition of PFOA or PFOS further amplified the emission. The enhancement was attributed to electrostatic and hydrophobic interactions between the fluorinated surfactants and the EB–CTAB complex, which stabilised the fluorophore and suppressed non-radiative relaxation. The fluorescence intensity increased linearly across 0.05–10 μM, and an LOD of 12.8 nM for PFOS and 11.8 nM for PFOA was reported. Application to environmental water samples yielded good precision, and RSDs of 4.3% and 2.9%, respectively.[106] Cheng *et al.* (2019) developed a dual-mode carbon dot (CD)-based fluorescence sensor that enabled both visual and spectroscopic detection of PFOS (Fig. 6b).[103] The fluorescence of CDs was initially quenched by berberine chloride hydrate (BH) through ground-state complex formation, electrostatic attraction, and an inner filter effect (IFE). Upon PFOS addition, preferential PFOS–BH binding disrupted the quenching, leading to fluorescence recovery at 448 nm and a pronounced enhancement at 533 nm. This dual-emission behaviour produced a visible colour shift from blue to pale yellow, enabling rapid visual confirmation. Under optimised conditions, the intensity at 533 nm exhibited a linear correlation with PFOS concentrations from 0.22 to 50.0 μM and an LOD of 21.7 nM was reported. The method was selective and capable of distinguishing PFOS from structurally related PFOA.[103]

He *et al.* (2020) proposed a chitosan-assisted fluorometric system for PFOS detection that eliminated the need for nanomaterial synthesis.[104] The approach employed a competitive "turn-on" mechanism in which the dye trisodium-8-hydroxypyrene-1,3,6-trisulfonate (HPTS) was initially quenched by protonated chitosan through electrostatic interactions and photoinduced electron transfer. Introduction of PFOS resulted in stronger PFOS–chitosan interactions,

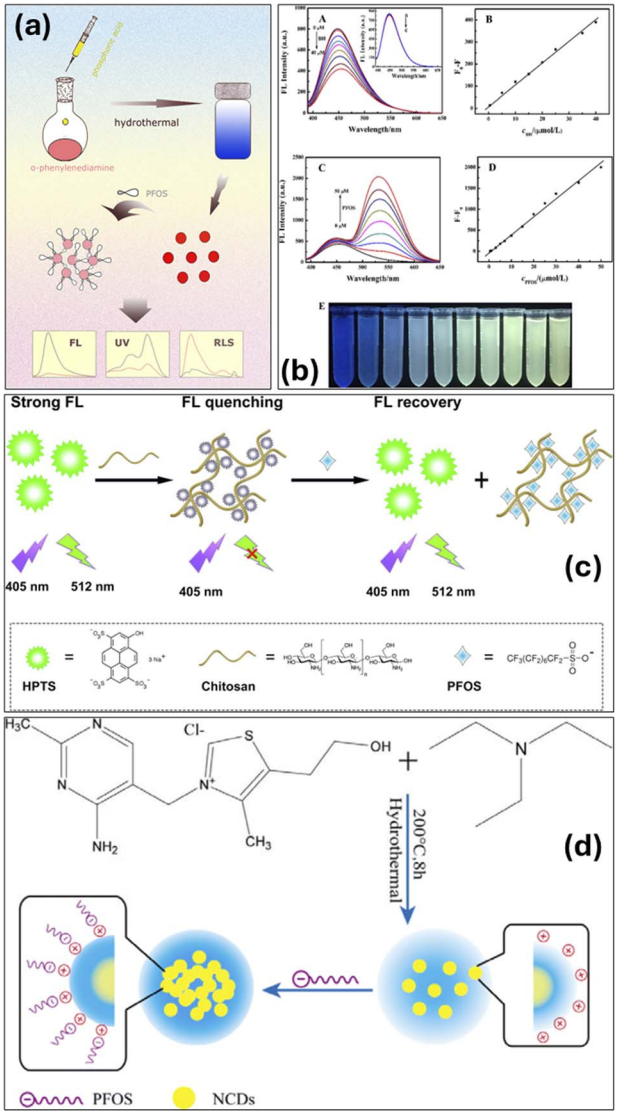

Fig. 6 (a) Schematic illustration of CDs-based triple-channel optical nanosensor for PFOS detection.[102] Reproduced from ref. 102 Copyright (2019) with permission from Elsevier. (b-A) Fluorescence emission spectra of CDs in the presence of BH at various concentrations of 0–40 μmol L^{-1}. The inset shows that the fluorescence spectra of CDs, CDs-PFOA and CDs-PFOS, respectively. (a) CDs-PFOS; (b) CDs; (c) CDs-PFOA. Concentration: CDs, 60 μL; PFOS, 5 μmol L^{-1}; PFOA, 5 μmol L^{-1}. (b-B) The corresponding calibration curve. F_0 and F are the fluorescence intensity of CDs in the absence and presence of BH. (b-C) Fluorescence emission spectra of CDs-BH in the presence of PFOS at various concentrations of 0–50 μmol L^{-1}. (b-D) The corresponding calibration curve. F_0 and F are the fluorescence intensity of CDs-BH in the absence and presence of PFOS. (b-E) The photo of FL color change of CDs/CDs-BH at various concentrations of PFOS. The concentrations of PFOS from left to right are 0, 0, 5, 10, 15, 20, 25, 30, 40 and 50 μmol L^{-1}, respectively.[103] Reproduced from ref. 103 Copyright (2019) with permission from Elsevier. (c) Schematic diagram of the fluorometric method based on CTS-mediated "turn-on" strategy for detection of PFOS.[104] Reproduced from ref. 104 Copyright (2020) with permission from Elsevier. (d) Graphical abstract: nitrogen-doped carbon dots as an effective fluorescence enhancing system for the determination of perfluorooctyl sulfonate.[105] Reproduced from ref. 105 Copyright (2019) with permission from Springer Nature.

displacing HPTS and restoring its fluorescence. The entire procedure was completed within 25 minutes, offering a rapid and efficient alternative to nanoparticle-based systems. The sensor exhibited a linear response over 0.0050–2.0 μM and exhibited an LOD of 1.0 nM, suggesting its potential for PFOS detection in environmental water samples (Fig. 6c).[104]

Another refinement of "turn-on" fluorescence sensing was demonstrated by Lin *et al.* (2019), who synthesised nitrogen-doped carbon dots (NCDs) *via* a hydrothermal route using vitamin B_1 and triethylamine as precursors.[105] NCDs exhibited strong fluorescence enhancement upon exposure to PFOS, driven by electrostatic attraction between the negatively charged PFOS molecules and the NCD surface. This interaction induced partial aggregation and reduced non-radiative energy dissipation, resulting in intensified emission. The system was reported to maintain selectivity in the presence of common metal ions, competing anions, and structurally similar surfactants. Under optimised conditions, a linear response was reported across 0.3–160 nM, with an LOD of 0.3 nM (Fig. 6d).[105] It was reported that the sensor performed reliably in real water samples, confirming its potential for environmental monitoring.[105]

Collectively, fluorescence strategies represent a versatile and highly sensitive platform for PFOS detection. Signal amplification in these systems arises primarily from analyte-induced modulation of the fluorophore environment, typically through electrostatic, hydrophobic, or competitive binding interactions that restore or enhance fluorescence. Their inherent sensitivity, selectivity, and operational simplicity highlight the promise of such techniques for rapid and cost-effective PFAS monitoring in environmental samples.

Table 4 provides an overview of fluorescence-based detection techniques for PFAS presenting key performance parameters and associated references.

4. Electrochemical sensor-based detection

Electrochemical sensing platforms have been found to garner significant interest for the purpose of environmental sensing, considering the various advantages that they provide over traditional analytical techniques. They are portable, cost-effective and simple in terms of their instrumentation and overall design. Electrochemical sensors are generally constructed by integrating a recognition material onto an electrode surface. This material is designed to interact specifically with the target analyte. When PFAS compounds come into contact with the sensing surface, they cause chemical or physical changes that are converted into electrical signals. These signals can then be measured to determine the presence and concentration of the PFAS contaminants.[116] The efficiency of an electrochemical sensor largely depends on the choice of materials and the recognition mechanism involved. Interactions between the target molecules and the sensor surface can lead to variations in electrical properties which are reflected in measurable outputs such as current, voltage, resistance, or impedance.[117] Despite the various advantages provided by

Table 4 Fluorescence based techniques for PFAS detection in various water samples

Detection technique	Analyte(s)	Sample type	Description/title	LOD	Range	Ref.
Fluorescent (turn off)	PFOS	River & tap water	A new dual-recognition strategy for hybrid ratiometric and ratiometric sensing perfluorooctane sulfonic acid based on high fluorescent carbon dots with ethidium bromide	27.8 nM	0–2.0 μM	94
	PFOA	Spiked textile samples (water)	Rapid fluorometric determination of perfluorooctanoic acid by its quenching effect on the fluorescence of quantum dots	0.3 μmol L^{-1}	0.5–40 μmol L^{-1}	101
	PFOS	River & tap water	A sensitive and selective triple-channel optical assay based on red-emissive carbon dots for the determination of PFOS	18.27 nmol L^{-1}	0.5–12 μmol L^{-1}	102
	PFOS	Stream water samples	Detection of PFOS and copper(II) ions based on complexation induced fluorescence quenching of porphyrin molecules	8.0 nM	0.05–16.0 μM	107
	PFOA	Lake & tap water and urine	Selenium and nitrogen co-doped carbon quantum dots as a fluorescent probe for perfluorooctanoic acid	1.8 μM	10–70 μM	108
	PFCPs	Tap, river, and surface seawater & food-packaging samples	Sensing of perfluorinated compounds using a functionalized tricolor upconversion nanoparticle based fluorescence sensor array	40 nM	—	109
	PFOS	Surface water (lake), human serum & egg extract	Fabrication of a near-infrared excitation surface molecular imprinting ratiometric fluorescent probe for sensitive and rapid detecting perfluorooctane sulfonate in complex matrix	1 pmol L^{-1}	0.001–0.1 nmol L^{-1}	110
	PFOS	Tap & river water samples	Surface molecular imprinting on dye–(NH_2)–SiO_2 NPs for specific recognition and direct fluorescent quantification of perfluorooctane sulfonate	5.57 μg L^{-1}	5.57–48.54 μg L^{-1}	111
	PFOA	Tap & river water samples	Core–shell quantum dots coated with molecularly imprinted polymer for selective photoluminescence sensing of perfluorooctanoic acid	25 nmol L^{-1}	0.25–15.00 μmol L^{-1}	112
Fluorescent (turn on)	PFOS, PFOA	Tap & river water samples	An erythrosin B-based “turn on” fluorescent sensor for detecting perfluorooctane sulfonate and perfluorooctanoic acid in environmental water samples	PFOS: 12.8 nM PFOA: 11.8 nM	0.05–10 μM	106
	PFOS	Tap & river water samples	Highly selective fluorescent visual detection of perfluorooctane sulfonate *via* blue fluorescent carbon dots and berberine chloride hydrate	21.7 nmol L^{-1}	0.22–50.0 μmol L^{-1}	103
	PFOS	River & lake water samples	A chitosan-mediated “turn-on” strategy for rapid fluorometric detection of perfluorooctane sulfonate	1.0 nmol L^{-1}	0.0050–2.0 μmol L^{-1}	104
	PFOS	River & lake water samples	Nitrogen-doped carbon dots as an effective fluorescence enhancing system for the determination of perfluorooctyl sulfonate	0.3 nM	0.3–160 nM	105

Table 4 (*Contd.*)

Detection technique	Analyte(s)	Sample type	Description/title	LOD	Range	Ref.
	PFAS: PFOA, PFOS, 6:2FTS	Milli-Q water (standard solutions)	Aggregated-fluorescent detection of PFAS with a simple chip	—	0.1–100 μM (PFOA)	113
	PFOS	River & tap water samples	An eosin Y-based "turn-on" fluorescent sensor for detection of perfluorooctane sulfonate	1.5×10^{-8} mol L^{-1}	0 to 2.0×10^{-6} mol L^{-1}	114
	PFOS	Deionised & tap water samples	Fluorescence detection of perfluorooctane sulfonate in water employing a tetraphenylethylene-derived dual macrocycle BowtieCyclophane	47.3 ± 2.0 nmol L^{-1} (DI); 77.8 ± 8.8 nmol L^{-1} (tap)	0–0.6 μmol L^{-1}	115

electrochemical sensing platforms, there are also some limitations which include the possibility of interference from complex matrices, electrode fouling, and overall stability/reproducibility of the sensor depending on the electrode material and the surface modification strategy employed. The adaptability and performance of electrochemical sensors make them increasingly favored over conventional methods. They offer high sensitivity and selectivity, and cost-effectiveness, which support their growing use in diverse areas including environmental surveillance, pharmaceutical residue monitoring, biomedical diagnostics, food quality control, and chemical manufacturing.[118] These sensors are particularly efficient at pinpointing specific target analytes in complex mixtures and achieve detection limits spanning a broad range from pg L^{-1} to μg L^{-1}, depending on the electrode material, surface modification strategy, and molecular recognition mechanism employed. This broad-range sensitivity positions them as highly effective tools for monitoring contaminants across diverse environmental and health contexts.[119]

The fundamental working mechanism of these sensors hinges on the manipulation of electrochemical reactions at the interface between the electrode and the solution, where the variation in the transfer of electrons causes a response signal. A standard configuration includes three distinct electrodes: a working electrode where the electrochemical event occurs, a reference electrode to maintain a stable potential, and a counter electrode that completes the circuit. The selection of materials for these electrodes and an in-depth understanding of the electrochemical and chemical interactions at the interface are pivotal for achieving reliable and selective detection.[130] Electrochemical sensors are broadly categorised based on their detection mechanism — potentiometric, amperometric, voltammetric and impedimetric, each offering a distinct transduction pathway that has been adapted for PFAS detection in complex environmental matrices.[38]

However, the detection of PFAS by electrochemical sensors is inherently challenging due to the weak or negligible intrinsic electroactivity of PFAS molecules, which cannot be directly oxidised or reduced at conventional electrode surfaces. To overcome this, indirect detection strategies are predominantly employed, wherein a modified electrode surface, typically functionalised with MIPs, nanomaterials, or aptamers, selectively captures PFAS molecules, causing measurable changes in current, impedance, or potential.[120,121] For MIP-based sensors, PFAS binding within the imprinted cavities restricts access of a redox probe (*e.g.*, ferrocenecarboxylic acid or $[Fe(CN)_6]^{3-/4-}$) to the electrode surface, producing a quantifiable signal decrease which is proportional to PFAS concentration. For impedimetric systems, analyte binding increases the interfacial charge-transfer resistance, which is measured by electrochemical impedance spectroscopy (EIS).[131]

A recent study introduced a bubble-nucleation-based electrochemical sensor that achieved a detection limit of about 30 μg L^{-1} for PFAS.[132] While this level remains above current regulatory thresholds, it demonstrates a creative sensing concept and provides a useful foundation for improving sensitivity to environmentally relevant concentrations (ng L^{-1})

Table 5 Electrochemical sensors for PFAS detection in various water samples

Sensor type	Analyte(s)	Sample type/source considered	Electrode or sensor description/platform	Detection technique	LOD	Ref.
MIPs based	GenX-HFPO-DA	River water	μ-MIP: MIP-modified Au microelectrode	DPV	250 fM	120
	PFOS	Distilled water, tap water, and bottled mineral water	Gold electrode modified with a thin coating of a MIP, prepared by anodic electropolymerization of *o*-PD	DPV	0.04 nM	121
	PFOS	River water	MIP-modified glassy carbon macroelectrode ($r = 1.5$ mm)	EIS	3.4 pM	122
	PFOA	Tap water, river water, & lake water	Molecularly imprinted ultrathin graphitic carbon nitride nanosheets (MIP@utg-C_3N_4/GCE)	Electrochemiluminescence (ECL)	0.01 ppb	123
	PFOS	Tap water, river water, & mountain water	Molecularly imprinted polymer modified TiO_2 nanotube arrays (MIP@TiO_2 NTAs)	Photoelectrochemical (PEC) detection	86 ng mL^{-1}	124
	PFOA, PFOS, 6 : 2 FTS	Aqueous solutions, supporting electrolytes: PBS, NH_4Cl, and K_2SO_4	Potentiometric detection of fluoro-surfactants formulated in aqueous film-forming foams (AFFFs): MIP formed on pencil lead. Methylene blue introduced into the polymer matrix of polypyrrole to increase the selectivity	Potentiometric detection	0.1 μM (~41 ppb) (PFOA)	125
	PFOSF	Tap water, river water & lake water	Functionalized screen-printed carbon electrode: integration of SPE, BiOINFs and MIPs (MIP@BiOINFs/SPE)	PEC detection	0.01 ppb	126
Immuno-sensors & others	PFOA	Phosphate buffer (no real water tested)	Covalent immobilization of delipidated human serum albumin on a poly(pyrrole-2-carboxylic) acid film—modified graphite screen-printed electrode (hSA-Py-2-COOH-G-SPE)	EIS (impedimetric detection)	Avg. Mean signal ($n = 5$) for buffer & PFOS lower than value obtained with 500 nM PFOA	127
	PFOA	Environmental water samples (river, lake & tap water)	PEC sensing platform: CuSe/CdSe/TiO_2 NTs composites as the photoactive material and an anti-PFOA aptamer as the biorecognition element	PEC detection	0.053 pg L^{-1}	128
	PFOS	Reservoir water & river water	Electrochemical biosensor based on inhibition biocatalysis of an enzymatic biofuel cell (BFC): the multi-walled carbon nanohorns modified GCE (MWNHs/GCE) was used as substrates for the bioanode and biocathode, and glutamic dehydrogenase (GLDH) & bilirubin oxidase (BOD) as biocatalysts for bioanode & biocathode	Open-circuit potential (V_{oc})	1.6 nmol L^{-1}	129

in future developments. Despite these promising developments, crafting electrochemical sensors that effectively detect PFAS compounds remains challenging. Nevertheless, continuing innovation in electrochemical methods has led to the emergence of advanced sensing platforms that address various challenges and obstacles. Techniques involving engineered electrode materials, such as carbon-based nanostructures, doped metal oxides, and hybrid nanocomposites, as well as the development of microelectrode arrays, have greatly enhanced sensitivity and broadened the scope of detectable analytes. These systems offer lower production costs, simplified operation, and superior analytical performance, making them ideal for monitoring a wide array of contaminants of emerging concern.[119]

The performance of electrochemical PFAS sensors, particularly MIP-based and immunosensor platforms, is critically influenced by the thermodynamics and kinetics of PFAS binding at the recognition layer. In MIP sensors, the binding of PFAS within imprinted cavities is governed by a combination of hydrophobic forces, electrostatic attraction, and geometrical complementarity; the resulting apparent dissociation constant determines the sensor's linear dynamic range and lower detection limit.[122] Competitive displacement by structurally similar PFAS, for instance, PFBS displacing PFOS from a sulfonate-imprinted MIP, reduces effective binding site occupancy and causes underestimation of target analyte concentration.[77] Ionic matrix components are particularly disruptive: elevated ionic strength (as found in seawater or wastewater) alters Debye screening of electrostatic interactions[133] and can cause MIP polymer swelling, shifting limits of quantification relative to clean buffer calibration standards.[134] For immunosensors, non-specific adsorption of matrix proteins and humic substances onto antibody-modified electrode surfaces causes elevated baseline impedance and a reduced dynamic signal range, effects that are typically managed through surface blocking with bovine serum albumin (BSA) or polyethylene glycol (PEG) coatings.[135] For all electrochemical formats, matrix-matched calibration, standard addition, or internal referencing strategies are recommended to achieve accurate quantification in complex environmental samples.

4.1. MIP based electrochemical approaches

Among the diverse electrochemical strategies developed for PFAS detection, MIPs have emerged as one of the most versatile and selective options. MIPs are synthetic recognition materials designed to replicate the unique structure, size, and functional characteristics of target molecules. During their synthesis, functional monomers, cross-linking agents, and initiators are polymerised in the presence of the analyte. Once polymerisation is complete, removal of the template leaves behind molecular cavities that are complementary in size, shape, and chemical functionality to the target PFAS. These tailored binding sites allow the polymer to selectively rebind the analyte, producing measurable electrochemical signals through changes in current, potential, or impedance.[121] Acting as artificial receptors, MIPs combine the specificity of biological molecules with the durability and tunability of synthetic materials. Their robustness, reusability, and cost-effectiveness, together with their straightforward fabrication, make them particularly attractive for portable PFAS sensors.[136–138] Additionally, their surface chemistry can be easily tailored, enabling selective detection in complex environmental matrices where interfering species are common.

In the reported electrochemical sensing systems, MIPs have been combined with electrochemical transduction methods such as voltammetry, amperometry, or impedance spectroscopy, in which the binding of the target at the MIP sites generates an electrical response. These systems have shown promising analytical characteristics, including detection limits, selectivity towards the target PFAS, and the capacity for analysis at environmentally relevant concentrations. Moreover, electrode miniaturisation and potential for portability indicate promising prospects for the MIPs application for PFAS analysis. However, the problems of leakage, low efficiency of MIPs (for certain PFAS) and MIP optimisation need to be addressed.

Karimian *et al.* (2018) introduced a distinct electrochemical sensing approach capable of detecting ultra-trace levels of PFOS in both bottled and tap water samples.[121] Their design utilised a gold electrode surface modified with a MIP layer. This MIP was synthesised through the anodic electro-polymerisation of *o*-phenylenediamine (*o*-PD), with PFOS molecules acting as the template during polymer formation. After polymerisation, the PFOS templates were selectively removed using an optimised solvent system, generating recognition sites complementary in shape and chemistry to PFOS. The detection mechanism involved ferrocenecarboxylic acid (FcCOOH), an electroactive probe that competes with PFOS for access to the imprinted sites. The resulting sensor demonstrated impressive analytical performance, exhibiting high sensitivity and reproducibility, along with strong selectivity for PFOS. It achieved a low LOD of 0.04 nM, in close agreement with values obtained by HPLC-MS/MS.

Chen *et al.* (2015) designed a highly sensitive signal-off electrochemiluminescence (ECL) sensor employing a MIP@utg-C_3N_4-modified glassy carbon electrode.[123] In this system, specific recognition between the MIP and PFOA led to the entrapment of the analyte on the electrode surface.[123] The bound PFOA was subsequently oxidised by sulfate radicals (SO_4^{2-}), and this process consumed the radicals responsible for light emission, resulting in a measurable decrease in the ECL signal. The observed reduction in luminescence provided a direct quantitative measure of PFOA concentration. The study reported an LOD of 0.01 ppb, comparable to the sensitivity typically reported for LC-MS/MS analyses. Beyond its sensitivity, the authors reported high accuracy when tested with real water samples, confirming its practical applicability for environmental monitoring. It is worth noting that this approach combines high analytical performance with simplicity and low cost, highlighting the growing potential of MIP-based electrochemical systems for real-world PFAS detection. Notably, Moro *et al.* (2019) reported an electrochemical MIP sensor for PFOS using a gold screen printed electrode (ScPE), offering a portable and low-cost platform with sufficient conductivity and stability for miniaturised systems.[139]

Glasscott *et al.* (2020) developed another electrochemical sensor for PFAS quantification.[120] They presented a MIP-modified microelectrode ($r = 6.25$ μm) sensor for quantifying the pervasive environmental PFAS GenX (HFPO-DA) in surface water. The microscale electrode was generated through anodic electropolymerisation of o-PD (20 nm) in the presence of GenX, resulting in a templated polymer adjacent to the electrode surface. Subsequent solvent extraction yielded GenX-specific recognition sites. The sensor showed an LOD of 250 fM, with a linear detection range of 1−5000 pM (Fig. 7 Top).[120] Gong *et al.* (2015) developed a rapid and ultrasensitive signal-off photoelectrochemical sensor under visible-light irradiation for PFOA detection in real water samples.[140] A nanostructured probe composed of MIP – modified with AgI nanoparticles–BiOI nanoflake arrays (AgI–BiOINFs) was designed as the photoactive electrode, denoted as MIP@AgI–BiOINFs. The conduction band (CB) level of AgI (∼−0.55 eV) is positioned more negatively than that of BiOINFs (0.58 eV), enabling facile injection of photogenerated electrons from AgI into the CB of BiOINFs. These electrons then transfer to the external circuit *via* the conductive FTO substrate. Concurrently, the holes residing in the valence band (VB) of BiOI (∼2.39 eV) migrate to that of AgI (∼2.25 eV). This orchestrated charge transfer effectively mitigates electron-hole pair recombination, promoting the efficient separation of photogenerated carriers. The sensor exhibited a linear range of 0.02–1000.0 ppb with a reported LOD of 0.01 ppb, comparable to LC-MS/MS (Fig. 7, bottom).[140]

Kazemi *et al.* (2020) developed a MIP-based electrode to detect PFOS and reported an LOD of 0.05 nM.[141] MIPs were formed by the anodic deposition of *o*-PD in the presence of PFOS template molecules on a glassy carbon macroelectrode. The performance of the resulting MIP electrode was evaluated by using the current obtained from the oxidation of ferrocene carboxylic acid as the electrochemical probe. To better understand PFOS association with the MIP, a Langmuir binding model was reported to be developed based on the changes in electrochemical responses of the MIP. Fitting the model to the experimental data gave an association constant (K_A) of 4.95×10^{12} over a PFOS concentration range of 0 to 0.05 nM.[141] Moro *et al.* (2020) designed an impedimetric electrochemical sensor by covalently attaching delipidated human serum albumin (hSA) onto pyrrole-2-carboxylic acid (Py-2-COOH) on a graphite ScPE.[127] The ease of combining protein bioreceptors with Py-2-COOH-G-SPE for PFOA monitoring in water samples was reported in this proof-of-concept study.

Overall, MIP-based electrochemical sensors show considerable promise for PFAS detection, offering excellent selectivity, reproducibility, and adaptability. Their sensing mechanisms typically involve electroactive probes or signal modulation processes that respond to competitive binding at the imprinted recognition sites. These analyte–polymer interactions produce measurable electrochemical or photoelectrochemical signals, providing a direct link between molecular recognition and sensor response. By judiciously selecting functional monomers and optimising polymerisation conditions, MIPs can be tailored to reach ultra-trace detection limits, sometimes even surpassing those obtained by conventional analytical methods such as LC-MS/MS. Importantly, their simple fabrication, low cost, and compatibility with miniaturised electrodes make them highly suitable for on-site PFAS analysis and routine environmental monitoring applications.

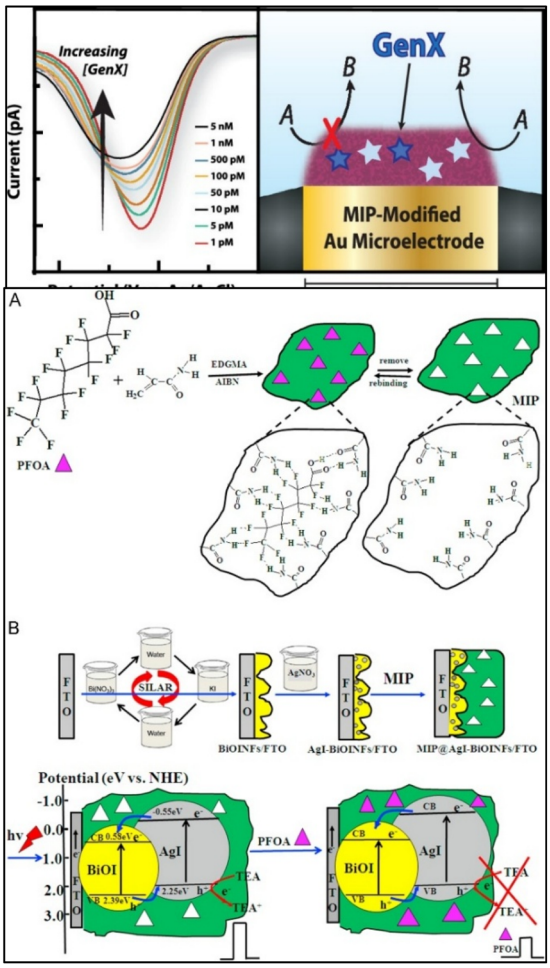

Fig. 7 Top: μ-MIP: Molecularly imprinted polymer-modified microelectrodes for the ultrasensitive quantification of GenX (HFPO-DA) in river water (Abstract).[120] Reproduced from ref. 120 Copyright © 2020 American Chemical Society. This is an open access article published under an ACS AuthorChoice License (https://pubs.acs.org/page/policy/authorchoice_termsofuse.html). Bottom: Schematic illustration of the formation process of (A) the MIP, and (B) the SILAR deposition of AgI–BiOINFs films as well as the principle of PEC determination of PFOA using MIP@AgI–BiOINFs/FTO.[140] Reproduced from ref. 140 Copyright (2015) with permission from Elsevier.

4.2. Electrochemical immunosensors and others

Immunoassay-based strategies have gained considerable attention owing to the intrinsic specificity of antibody–antigen interactions. These approaches represent a bio-recognition-driven analytical technique that utilises highly selective binding between antibodies and target analytes to enable sensitive detection of specific compounds within complex matrices. Immunosensors, which integrate these recognition events with electrochemical signal transduction, offer a sensitive and selective route for PFAS detection in diverse aquatic

systems.[119] Typically, antibodies or analogous recognition elements are immobilised on an electrode surface, and binding between the target analyte and antibody induces measurable variations in current, potential, or impedance that can be quantified electrochemically. This approach enables rapid analysis with less complex equipment than is needed for conventional chromatography, and several studies have shown that low detection limits for PFAS compounds can be achieved with electrochemical immunosensing. Despite their high sensitivity and potential for miniaturisation, challenges still exist. These include the limited availability of highly selective antibodies for the numerous PFAS compounds, the possibility of cross-reactivity between PFAS compounds that have similar structures, and the requirement for sensor surface modification.

Beyond antibody-based recognition, alternative biomolecular probes have also been explored. Notably, delipidated hSA was employed as a binding element to enhance PFOA recognition. Upon exposure to PFOA, the sensor exhibited a measurable increase in impedance, whereas PFOS generated only a partial response that was not systematically investigated over a concentration range.[127] This label-free, protein-based sensing approach underscores the potential of naturally abundant biomolecules in PFAS detection. However, further validation remains necessary to confirm reproducibility, selectivity, and applicability in complex environmental matrices. Additional electrochemical biosensing platforms have also been investigated, including enzyme-modified electrodes, protein-functionalised interfaces, and bioassay-integrated systems.[142,143] Aptamers have also been explored due to their specificity and high binding affinity. An efficient photoelectrochemical sensing platform using CuSe/CdSe/TiO_2 nanotube composites and an anti-PFOA aptamer was reported for highly sensitive detection, achieving a very low LOD of 0.053 pg L^{-1}.[128]

Each of these provides complementary advantages for PFAS analysis and broadens the scope of electrochemical detection beyond MIP- and antibody-driven mechanisms. Taken together, these electrochemical sensors represent a promising frontier for PFAS monitoring. Their combination of high sensitivity, molecular selectivity, and adaptability supports rapid, on-site detection of environmental samples. With ongoing advances in recognition chemistry, nanomaterial-assisted amplification, and electrode miniaturisation, these platforms are poised to become practical tools for routine water quality assessment and regulatory monitoring. A comparative summary of electrochemical sensor performance for PFAS detection in various water samples is presented in Table 5.

5. Electrophoresis (separation-based) methods

Unlike the sensor-based platforms described in Sections 3 and 4, electrophoresis is primarily a separation technique that resolves structurally similar PFAS prior to detection by a coupled detector such as UV absorbance or mass spectrometry. Capillary electrophoresis (CE) is an analytical technique for separating charged species in a narrow capillary under the influence of a high-voltage electric field. Separation is achieved based on differences in electrophoretic mobility (a function of the ratio of charge to hydrodynamic size of the analytes) as well as possible interactions with the background electrolyte. Since many of the PFAS compounds are ionisable under analytical conditions, electrophoresis is an efficient method for separating structurally similar PFAS homologues and isomers prior to detection. The technique has several advantages, such as high resolution, short analysis time, and extremely low solvent consumption compared to conventional chromatographic techniques. However, it is mostly used with UV or mass spectrometric detection, as electrophoresis is for separation and not identification of the species.

Early studies demonstrated that CE could resolve perfluoroalkyl acids by exploiting their anionic character, though detection was initially challenging because PFAS lack strong chromophores. Wójcik *et al.* (2005) developed one of the first capillary zone electrophoresis methods for perfluorocarboxylates, separating C6–C12 PFCAs with both direct UV detection at 190 nm and indirect UV detection using an added chromophore.[144] Optimal separation was achieved with a phosphate buffer containing 40% isopropanol, and on-line sample stacking was explored to boost sensitivity. However, detection limits remained unsatisfactory, reflecting the inherent sensitivity limitations of UV detection for PFAS. In a follow-up study, Wójcik *et al.* (2006) improved the method by employing indirect photometric detection with 2,4-dinitrobenzoic acid as a UV-absorbing probe in the background electrolyte.[145] This refined CE protocol (50 mM Tris, 50% methanol, pH 9.0) achieved baseline separation of C6–C12 PFCAs within ~20 minutes and lowered LODs to 0.6 to 2.4 mg L^{-1}.[145] These early developments confirmed the feasibility of CE for PFAS analysis in water but also highlighted the need for better sensitivity and selective detection. Subsequent methodological advances addressed these limitations. A key challenge was the poor resolution of long-chain PFAS (PFOA and PFOS) under fully aqueous conditions.

CE separates PFAS based on differences in charge-to-hydrodynamic-radius ratios, providing speciation complementary to reversed-phase LC. Long-chain PFAS homologues (*e.g.*, C6–C12 PFCAs) can be resolved as a function of chain length because electrophoretic mobility decreases systematically with increasing chain length in a given background electrolyte.[145] However, ionic matrix components (*e.g.*, chloride, sulfate, and carbonate) that dominate environmental water samples can suppress or distort electrophoretic peaks by disrupting background electrolyte conductivity; on-line preconcentration strategies such as field-amplified sample injection (FASI) and large-volume sample stacking (LVSS) partially mitigate these effects while simultaneously improving sensitivity.[146]

These principles were concurrently demonstrated by Knob *et al.* (2012), who showed that PFOA and PFOS, which co-migrate under all tested aqueous background electrolyte conditions (pH 2–9), can be baseline-resolved using non-aqueous capillary electrophoresis (NACE), exploiting differences in ion-solvent interactions unavailable in aqueous

media.[147] A background electrolyte of 5 mmol L^{-1} naphthalene-1-sulfonic acid and 10 mmol L^{-1} triethylamine dissolved in ACN : MeOH (50 : 50, v/v) in an uncoated fused-silica capillary provided optimal separation and detection conditions. On-line preconcentration was subsequently applied: LVSS improved LODs by 69-fold (PFOA) and 143-fold (PFOS), while FASI delivered a further enhancement of 624-fold and 806-fold, respectively, achieving LODs of 31 nM for PFOA and 40 nM for PFOS (~13–22 ppb).[147] Combined with off-line solid-phase extraction of river water, the method achieved sub-nanomolar detection (~10^{-10} M, ~0.2–0.3 ppb), making it suitable for trace contamination screening in environmental water samples. Together, these results establish NACE with staged preconcentration as a viable CE strategy for trace PFAS screening in environmental matrices, despite the traditionally weaker sensitivity of CE relative to LC-MS methods.[147]

Another development in electrophoretic PFAS analysis is the use of contactless conductivity detection with CE, which skips the need for optical or MS-based detection and is amenable to field deployment. Lees *et al.* (2020) implemented a fast nonaqueous CE method with contactless conductivity detection to separate multiple PFAS within 5 minutes.[148] By employing a background electrolyte of 3-(*N*-morpholino)propanesulfonic acid (MOPS) and triethylamine in a 50 : 50 methanol–acetonitrile mixture, they achieved efficient separation of perfluoroheptanoate, PFOA, and PFOS as distinct, sharp peaks. The method showed a good linear response (R^2 > 0.996) in the low micromolar range and provided detection limits of approximately 0.30–0.75 μM for these analytes with a simple injection.[148] While these LODs (on the order of 0.1 ppm) are higher than those attained by mass spectrometry, the strength of the approach lies in its simplicity and speed. Importantly, after a pre-concentration step (solid-phase extraction of water samples), the effective detection limits were improved to 0.1–0.4 nM. This brought the sensitivity into the parts-per-trillion range, demonstrating that CE with conductivity detection can handle trace-level PFAS in complex matrices such as wastewater when coupled with sample cleanup. The authors highlighted the potential for this NACE-conductivity platform to be adapted into a portable format, enabling on-site PFAS monitoring in environmental samples. Such advances broaden the accessibility of electrophoretic methods beyond the traditional laboratory setting.

Coupling capillary electrophoresis to mass spectrometry (CE-MS) has further enhanced the detection capabilities for PFAS, combining the high resolving power of CE with the sensitivity and selectivity of MS detection. Historically, CE-MS for anionic pollutants suffered from sensitivity losses due to the necessity of sheath liquid interfaces, which dilute the analyte stream. Recent interface innovations aim to minimise this dilution. Höcker *et al.* (2020) developed a nanoflow sheath-liquid electrospray ionisation (ESI) interface for CE-MS that significantly improved concentration sensitivity for PFAS analysis.[149] In their approach, a bare-fused silica capillary CE was coupled to a high-resolution Orbitrap mass spectrometer *via* a tapered nanospray emitter, allowing stable electrospray at nL min^{-1} flow rates. An optimised low-pH, partially organic electrolyte (10% acetic acid with 10% 2-propanol) and the use of large-volume sample injection were critical for achieving both separation and detection of highly polar PFAS that are poorly retained by LC. This CE–nanoESI-MS setup achieved sub-ppb quantification limits for target analytes, on par with conventional LC-MS methods. In fact, LOQs of around 0.1–0.5 μg L^{-1} were reported for PFOA and PFOS in drinking water, with excellent linearity (R^2 > 0.993) and fair reproducibility (≈14% RSD in peak areas) given the low concentrations. Notably, the method required no sample pre-concentration or extraction: it was applied directly to chlorinated drinking water samples, and detected PFOA, PFOS, trifluoromethanesulfonate and various halogenated acetic acids at levels ranging from ~0.1 to 6 μg L^{-1}. The successful identification of these trace contaminants and additional suspect PFAS (*e.g.*, halogenated methanesulfonic acids) showcases the power of modern CE-MS for broad-spectrum screening. This work reports a significant leap in overcoming the sensitivity barrier of CE, demonstrating that, with refined interfaces and high-resolution MS, even ultra-trace detection of PFAS in complex environmental matrices is attainable by electrophoretic means.[149]

Beyond environmental monitoring, electrophoresis-based methods have been adapted for human biomonitoring and exposure studies, as demonstrated by their application to PFAS quantification in biological fluids such as serum. Azab *et al.* (2020) introduced a high-throughput CE-MS/MS strategy for biomonitoring PFAS in human serum, leveraging a technique called multisegment injection (MSI) to increase sample throughput.[150] In MSI-CE, multiple sample plugs are injected sequentially in a single run, separated by buffer segments, allowing parallel analysis of several samples. Here, MSI with a nonaqueous CE separation was implemented and interfaced with tandem mass spectrometry (negative-mode electrospray with multiple reaction monitoring) for specific quantification of PFOA and PFOS in serum extracts.[150] A simple liquid–liquid extraction with methyl *tert*-butyl ether was sufficient for sample preparation, and the electrophoretic separation of PFOA/PFOS was accomplished within 3 minutes per sample segment. Despite the high throughput, the method maintained adequate sensitivity: LODs were in the order of 20 nM for both PFOA and PFOS, and linear calibration was achieved in the low nanomolar range. The authors improved quantitative precision by incorporating an internal standard and optimising a coaxial sheath-liquid ESI interface, yielding a mean coefficient of variation of ~9% over 84 injections. When applied to serum samples (n = 16), MSI-NACE-MS/MS measured median concentrations of ~3.3 nM for PFOA and PFOS (with ranges of 0.7–9.0 nM and 1.5–6.6 nM, respectively). These values were notably lower than those reported in older cohort studies (pre-2009), aligning with the phase-out of certain PFAS and validating the method's applicability to real-world exposure assessment.[150]

Electrophoresis-based methods for PFAS have seen marked advancements in the past two decades. Early CE approaches established the foundation for PFAS separation but were constrained by limited detection sensitivity.[144,145] Innovations such as nonaqueous electrolytes, indirect or contactless detection, on-line stacking, and multisegment injection have substantially

Table 6 Electrophoresis based PFAS analysis of various water samples

Analyte(s)	Sample type	Detection method	Electrolyte/medium	Detection limits (LOD/LOQ)	Ref.
C6–C12 PFCAs (incl. PFOA)	Aqueous solutions	CZE with (i) direct UV detection at 190 nm or (ii) indirect UV detection at 280 nm using 3,5-DNBA chromophore; fused-silica capillary, 75 μm ID	(i) 50 mM phosphate buffer + 40% isopropanol, pH 9.5 (direct UV detection) (ii) 5 mM 3,5-DNBA in 20 mM phosphate buffer, pH 9.3 (indirect UV detection)	LOD (PFCAs, direct UV): 2–33 μg mL^{-1} (C6–C12)	144
C6–C12 PFCAs (incl. PFOA)	River water, lake water, and tap water (spiked/fortified)	CZE with indirect UV detection at 270 nm using 2,4-DNBA chromophore; fused-silica capillary, 75 μm ID, 60 cm	Indirect UV detection: 2,4-DNBA for PFCAs (C6–C12) in water. Optimal analyte resolution & detection sensitivity: 50 mM Tris solution (pH 9.0) & 50% methanol (BGE)	LOD: 0.6 to 2.4 μg mL^{-1} (ppm)	145
PFOS and PFOA	River water (treated with SPE)	Nonaqueous capillary electrophoresis with indirect UV detection (214 nm); on-line preconcentration by FASI	5 mM naphthalene-1-sulfonic acid (NSA) and 10 mM triethylamine (TEA) in ACN/MeOH (50 : 50 v/v); pH_{app} 9.2	PFOS (FASI + SPE): LOD: 5.6×10^{-10} mol L^{-1} LOQ: 7.9×10^{-10} mol L^{-1} PFOA (FASI + SPE): LOD: 4.7×10^{-10} mol L^{-1} LOQ: 6.4×10^{-10} mol L^{-1}	147
PFHpA, PFOA and PFOS	Wastewater samples (treated by SPE)	Nonaqueous capillary electrophoresis with conductivity detection; SPE-NACE-CD method	0.75 mM MOPS and 1.5 mM TEA in acetonitrile : methanol (50 : 50, v/v)	MDL: 0.3 nM (PFHpA), 0.4 nM (PFOA), 0.1 nM (PFOS)	148
PFOA and PFOSA	Drinking water (no SPE; enrichment-free, direct injection)	CE coupled with high-resolution Orbitrap MS *via* a nanoflow sheath liquid interface (CE-HRMS); large-volume stacking injection	Bare fused-silica capillary; 10% acetic acid with 10% isopropanol	LOQ: 0.04 μg L^{-1} (PFOA) 0.4 μg L^{-1} (PFOSA)	149
PFOA and PFOS	Human maternal serum (after MTBE liquid extraction; 40-fold enrichment)	MSI-NACE-MS/MS; MRM negative ion mode; coaxial sheath liquid ESI; 7 samples/run (3 min per sample)	Bare fused-silica capillary; 35 mM ammonium acetate in ACN : MeOH : IPA: residual water (70% : 15% : 5% : 10%, v/v), apparent pH 9.5 (adjusted with NH_4OH)	LOD: 20 nM (PFOA) & 25 nM (PFOS); LOQ: 103 nM (PFOA) & 117 nM (PFOS)	150

lowered detection limits and improved throughput.[147,148] Coupling CE with modern mass spectrometry, especially using nano-ESI interfaces, has largely overcome past sensitivity limitations, enabling detection of sub-ppb PFAS levels in complex environmental waters and biological fluids.[149,150] These methodological developments broaden the analytical toolbox for PFAS, offering high-efficiency separation and complementary selectivity to traditional LC-MS techniques. Table 6 summarises electrophoresis-based methods for PFAS detection/quantification in water samples, covering the key parameters and associated references.

A comparative assessment of PFAS detection methods reveals critical trade-offs between analytical rigour, cost, and field deployability. Chromatographic methods, particularly LC-MS/MS, deliver the highest sensitivity and multi-compound speciation capability but remain confined to centralised laboratories due to high instrumentation and operational costs, extensive sample preparation requirements, and the need for skilled personnel. Optical and electrochemical sensors offer substantially lower costs, minimal sample preparation, and compatibility with portable hardware, making them more attractive for field deployment. Their selectivity in complex environmental matrices and long-term stability remain challenges to be addressed. Biosensor (aptasensors or immunosensors) based platforms achieve exceptional selectivity through biorecognition elements such as aptamers and antibodies, but issues of shelf life, reproducibility and scalability currently limit their routine application. Electrophoresis-based methods provide a middle ground, offering good separation efficiency with moderate portability. Taken together, these complementary strengths suggest that hybrid deployment strategies, combining laboratory-based confirmation with field-deployable rapid sensors, represent the most practical and cost-effective pathway for comprehensive PFAS monitoring.[13,151,152]

6. Future perspectives

Detecting PFAS in water remains a formidable challenge. These substances occur at ultra-trace levels (often below parts-per-trillion) and include diverse chemical structures with varying chain lengths and functional groups. Sensors and methods must meet extremely high sensitivity requirements, accommodate broad analyte diversity, and tackle complex sample matrices (natural organic matter, salts, *etc.*) that can mask PFAS signals. Currently, the limited availability of highly specific receptors means that many sensor designs have detection limits above the desired level or require labour-intensive preconcentration steps. Each detection platform discussed offers distinct strengths, yet each carries trade-offs in sensitivity, selectivity, portability, or matrix tolerance that restricts their standalone use for routine PFAS monitoring in complex environmental matrices.[153]

Chromatographic techniques, particularly LC-MS/MS, remain the gold standard for sensitivity and specificity but are fundamentally constrained by cost, infrastructure, and lack of portability. The state-of-the-art optical or electrochemical probes require sample extraction to reach low ppb levels.[154] The fundamental limitations such as low analyte binding affinity, slow diffusion and weak signals must be overcome to meet emerging regulatory benchmarks. Moreover, interferences from other water constituents can produce false positives or suppress the PFAS response, therefore improving specificity and robustness remains a critical priority. Colorimetric and fluorescence sensors offer operational simplicity and field deployability, but their susceptibility to matrix interference, modest selectivity among structurally similar PFAS congeners, and detection limits that typically remain in the low $\mu g\ L^{-1}$ range limit their standalone utility for regulatory compliance monitoring. Electrochemical sensors, particularly MIP-based impedimetric platforms are reported to be promising, as they are cost-effective and compatible with miniaturised electronics, while remaining amenable to surface engineering for selectivity enhancement.[155] Aptamer-based electrochemical sensors are another emerging direction, offering tunable binding affinity and regenerability. However, the field as a whole suffers from a critical gap, *i.e.* the vast majority of reported sensors are validated only against spiked laboratory standards, with very few demonstrating reliable quantification in certified reference matrices or against regulatory methods.[156] This validation deficit represents a critical priority for effective development of sensors capable of detecting the full structural diversity of PFAS, including ultra-short-chain and zwitterionic species that remain largely unaddressed by current platforms.

Looking forward, new sensing strategies promise to transcend these constraints. In particular, nanomaterial-enabled sensors are proving to be promising. Nanostructured surfaces (carbon nanotubes, graphene/MXene derivatives, metallic nanoparticles, *etc.*) dramatically increase electrode surface area and can be functionalised for PFAS affinity. For example, gold nanoparticles have been widely used in colorimetric PFAS assays because their aggregation can be tuned by PFAS interactions, producing a distinct colour change.[154] Other optical approaches, such as SERS or fluorescent assays, exploit the unique chemistry of PFAS headgroups and chains to produce highly sensitive readouts. Likewise, advanced electrochemical sensors are incorporating nanomaterial coatings or redox labels to achieve sub-ppb sensitivity. These devices are miniaturised and inexpensive, suggesting the possibility of disposable 'dipstick' probes or smartphone-read formats. In all cases, nanomaterial architectures tend to exhibit enhanced sensitivity and improved signal-to-noise ratios compared to bulk sensors, moving closer to the sub-ppb detection targets.

Another exciting trend is the development of hybrid biorecognition schemes. Instead of relying on a single recognition element, researchers are combining multiple selective materials on the same sensor. For instance, MIPs can be paired with biomolecular capture elements (aptamers or enzymes) on the same device. These hybrid MIP–aptamer sensors merge the strengths of both components. Recent reports show that such dual-recognition (hybrid) systems can achieve high sensitivity, low limit of detection, high stability under harsh environmental conditions, as well as high binding affinity, and superior selectivity compared to either element alone.[157] In practice, an aptamer provides rapid, reversible binding to a PFAS headgroup, while the surrounding MIP matrix enforces shape

selectivity and chemical confinement. Similarly, enzymes that degrade or transform PFAS (*e.g.* P450-type monooxygenases) could be integrated with polymer receptors to create self-amplifying sensors. By layering these complementary recognition motifs, sensors become more robust to interferents and more discriminating among PFAS analogues, pushing LODs ever lower.

Beyond individual sensor performance, future platforms will also emphasize multiplexed and smart detection. A practical water monitoring device should ideally measure PFAS along with co-contaminants (heavy metals, nitrates, and pesticides) in a single run. Multiplexed sensor arrays or microfluidic chips can accomplish this by spatially arraying different receptors. For example, recent microfluidic studies note that simultaneously detecting multiple analytes could bring substantial economic and resource benefits for environmental monitoring.[158] A single chip might have distinct channels or electrodes, each coated with a different PFAS-targeting MIP or aptamer, alongside sensors for metals or nutrient ions. Alternatively, patterned paper-based or polymer strips could include colorimetric test spots for PFAS and for nitrite or chromium in parallel. Such multi-analyte devices would enable comprehensive snapshots of water quality without the need for multiple separate tests. In field deployments, these multiplex platforms could continuously screen for PFAS in the context of overall contamination, providing cross-validation and helping to identify sources of mixed pollution.

Data analysis is another dimension where innovation will transform PFAS sensing. The sheer volume and complexity of data from distributed sensor networks call for AI and ML tools.[153] AI algorithms can detect subtle patterns or anomalies in sensor output that escape thresholding. For instance, a network of IoT-connected sensors could stream high-frequency time-series data on PFAS indicators; ML models (*e.g.* deep neural nets or convolutional networks) could then distinguish true contamination events from noise or drift. Recent work on water quality monitoring demonstrates that IoT-based anomaly detection systems can fuse diverse sensor inputs (pH, turbidity, ion sensors, *etc.*) to quickly flag irregularities.[159] By applying these techniques to PFAS sensors, the system could recognize transient spikes (*e.g.* industrial discharge) or long-term baseline shifts (*e.g.* seasonal variation). Pattern-recognition methods could also correlate sensor signals across multiple platforms (electrochemical and optical) to enhance reliability. In short, AI-assisted analysis and cloud connectivity turn raw sensor readings into actionable information, enabling automated alerts for compliance breaches or public health officials.

Integration with wireless communication and IoT is likewise poised to expand. Mobile platforms (smartphones and single-board computers) now play dual roles as both measurement devices and data hubs. For example, a colorimetric test strip analysed with a phone camera (Fang *et al.*) allowed on-site PFOA quantification with an LOD of ~0.5 ppb.[93] Although this detection limit still exceeded the strictest PFAS guidelines, it illustrated how everyday electronics can democratise sensing. Beyond manual readout, 'smart' PFAS sensors can directly upload results. Fibre-optic or printed sensors with miniaturised electronics (*e.g.* a Raspberry Pi or Arduino) can automatically digitize the refractive index or current changes and transmit them *via* cellular or Wi-Fi networks. Several groups are prototyping such systems; one recent design combined a surface-plasmon sensor (with a PFAS-selective MIP layer) with a microprocessor that streamed refractive-index data online.[38] In the future, deployment of numerous similar nodes could create sensor swarms or 'smart city' grids, filling in spatial and temporal gaps left by laboratory monitoring. Real-time mapping of PFAS levels, integrated into cloud platforms, would greatly enhance exposure assessment and remediation strategies.

Successfully translating recent advances in PFAS sensing into real-world applications requires attention to the technology-maturation pathway. The Technology Readiness Level (TRL) framework offers a useful structure for describing this progression, with early-stage laboratory demonstrations typically falling within TRL 2–4. Most emerging PFAS sensor concepts (including many electrochemical and optical designs) currently remain at this stage, where proof-of-concept has been shown but validation is limited to controlled laboratory conditions. Progressing toward TRL 6–7 requires systematic evaluation of practical deployment challenges, such as long-term sensor stability across variable water chemistries, mitigation of matrix interferences, robust calibration against established analytical methods (*e.g.*, LC-MS/MS), and integration into rugged housings suitable for field use. Achieving TRL 8–9 would involve full-scale pilot testing, third-party certification, and demonstration of reliable performance in operational environments such as drinking-water treatment plants or contaminated sites. For example, a laboratory-bench electrochemical PFAS probe at TRL $\approx$3 would need to advance through controlled pilot trials at a treatment facility (TRL 6–7) and undergo standardised performance evaluation before it could be considered a commercially viable technology. Viewing sensor development through this TRL-based lens helps establish realistic milestones such as demonstrating $\geq$90% agreement with reference methods across multiple field deployments and emphasises that scientific innovation must be matched by rigorous engineering, validation, and regulatory alignment.[160–162]

Next generation sensors must also address concerns about sustainability and regulatory alignment. Ideally, a PFAS sensor would be fabricated from non-toxic materials that minimise environmental burden, whether through recyclability, reduced material consumption, or compatibility with green synthesis routes. This eco-conscious approach helps ensure that addressing PFAS contamination does not introduce new environmental burdens. Green fabrication methods, including water-based chemistries, organic binders, and minimal use of fluorinated reagents should be prioritised. At the same time, sensor designs must be aligned with evolving regulatory standards. For instance, the US EPA has established enforceable maximum contaminant levels (MCLs) for several PFAS, and new regulations are emerging worldwide. Sensors whose detection limits are far from these thresholds will have limited practical utility, underscoring the urgency of improving PFAS monitoring for public health

protection.[3] Thus, developers must calibrate devices to meet or exceed the regulatory requirements, and collaborate with agencies to validate the overall performance. In practice, this might mean interlaboratory comparisons or aligning sensor outputs with certified methods. Emphasising eco-friendly components and compliance-ready detection will smooth the path from R&D to field adoption.

Ultimately, these scientific and technological efforts must be embedded in a comprehensive interdisciplinary framework. Advances in PFAS sensing will demand close collaboration among chemists (to develop novel receptors), materials scientists (to engineer nanostructures and green substrates), electrical engineers (to miniaturise electronics and wireless units), and data scientists (to handle AI algorithms). Public health researchers and regulators should be involved early to guide target specifications (which compounds and concentration ranges truly matter) and to interpret data in a risk-assessment context. By breaking down silos, a more holistic approach to PFAS monitoring emerges. The goal is a virtuous cycle: as sensor networks generate real-time PFAS maps, epidemiologists and toxicologists can refine exposure models, which in turn inform sensor deployment strategies and standards. The payoff is significant, *i.e.* timely PFAS detection and granular PFAS data collection can help in protecting our global communities by bridging the gap between environmental surveillance and public safety.

Funding

No funding is involved or used in writing this review article.

Author contributions

Baljit Singh: conceptualization, data curation, investigation, validation, visualization, writing – original draft, writing – review & editing. Zina Fredj: data curation, validation, writing – review & editing. Rangasamy Savitha: data curation, investigation, validation, writing – review & editing. Abhijnan Bhat: data curation, investigation, validation, writing – original draft. Gayathree Thenuwara: investigation, writing – review & editing. Isha Dahiya: data curation, investigation, writing – original draft. Suneha Goswami: validation, writing – review & editing. Simrjit Singh: validation, writing – review & editing. Xolile Fuku: validation, writing – review & editing. All authors have read and agreed to the submission and publication of this manuscript.

Conflicts of interest

There are no conflicts to declare.

Abbreviations

AFFF	Aqueous film-forming foam
AIBN	Azobisisobutyronitrile
APTES	3-Aminopropyltriethoxysilane
AS	Anionic surfactant
AuNPs	Gold nanoparticles
BH	Berberine chloride hydrate
BOD	Bilirubin oxidase
CB	Conduction band
CDC	Centres for Disease Control and Prevention
CDs	Carbon quantum dots
CE	Capillary electrophoresis
CECs	Contaminants of emerging concern
CTAB	Hexadecyltrimethylammonium bromide
CZE	Capillary zone electrophoresis
DPV	Differential pulse voltammetry
EB	Erythrosine B
ECL	Electrochemical luminescence
EGDMA	Ethylene glycol dimethylacrylate
EIS	Electrochemical impedance spectroscopy
EPA	Environmental Protection Agency
ESI	Electrospray ionisation
EtFOSA	*N*-Ethyl perfluorooctane sulfonamide
FASI	Field-amplified sample injection
FcCOOH	Ferrocene carboxylic acid
FOSE	Perfluorooctane sulfonamidoethanol
FOSA	Perfluorooctane sulfonamide
FOSAA	Perfluorooctane sulfonamidoacetic acid
FRET	Fluorescence resonance energy transfer
FS	Fluorinated surfactant
FTO	Fluorine-doped tin oxide
FTOH	Fluorotelomer alcohols
FTAC	Fluorotelomer acrylate
FTMAC	Fluorotelomer methacrylate
FTOS	Fluorotelomer olefins
FTSA	Fluorotelomer sulfonic acid
GC	Gas chromatography
GCE	Glassy carbon electrode
GLDH	Glutamic dehydrogenase
HFPO-DA	Hexafluoropropylene oxide-dimer acid
HPLC	High-performance liquid chromatography
HSA	Human serum albumin
IFE	Inner filter effect
LED	Light-emitting diode
LLE	Liquid–liquid extraction
LOD	Limit of detection
LOQ	Limit of quantitation
LPE	Liquid-phase extraction
MBAS	Methylene blue active substances
MeFOSA	*N*-Methyl perfluorooctane sulfonamide
MPA	3-Mercaptopropionic acid
MS	Mass spectrometry
MSI	Multistage injection
MWNH	Multi-walled carbon nanohorn
NACE	Nonaqueous capillary electrophoresis
NCDs	Nitrogen-doped carbon dots
NF	Nanoflakes
o-PD	*o*-Phenylenediamine
OFS	Optical fibre sensors
PFAA	Perfluoroalkyl acid
PFAS	Per- and polyfluoroalkyl substances
PFBA	Perfluorobutanoic acid
PFBS	Perfluorobutane sulfonate
PFCA	Perfluoroalkyl carboxylic acid
PFDA	Perfluorodecanoic acid

PFDoA	Perfluorododecanoic acid
PFDoDA	Perfluorododecanedioic acid
PFDoS	Perfluorododecane sulfonic acid
PFHA	Perfluoroheptanoic acid
PFHxA	Perfluorohexanoic acid
PFHxDA	Perfluorohexadecanedioic acid
PFHxI	Perfluorohexyl iodide
PFHxS	Perfluorohexane sulfonate
PFNA	Perfluorononanoic acid
PFOA	Perfluorooctanoic acid
PFODA	Perfluorooctadecanoic acid
PFOF	Perfluorooctyl fluoride
PFOI	Perfluorooctyl iodide
PFOS	Perfluorooctane sulfonate
PFOSF	Perfluorooctanesulfonyl fluoride
PFPeA	Perfluoropentanoic acid
PFTeDA	Perfluorotetradecanedioic acid
PFTA	Perfluorotetradecanoic acid
PFTrDA	Perfluorotridecanedioic acid
PFUnA	Perfluoroundecanoic acid
PFUnDA	Perfluoroundecanedioic acid
PEG	Polyethylene glycol
POF	Plastic optical fibre
POPs	Persistent organic pollutants
QDs	Quantum dots
QTOF	Quadrupole time-of-flight
RGB	Red–green–blue
RLS	Resonance light scattering
RSD	Relative standard deviation
S/N	Signal-to-noise ratio
ScPE	Screen printed electrode
SDVB	Styrene-divinyl benzene
SERS	Surface-enhanced Raman scattering
SPE	Solid-phase extraction
SPR	Surface plasmon resonance
TEA	Triethylamine
TEOS	Tetraethoxysilane (crosslinker)
TMB	3,3′,5,5′-Tetramethylbenzidine
TRLs	Technology readiness levels
UCNPs	Upconversion nanoparticles
UPC^2	Ultra-performance convergence chromatography

Data availability

No primary research results, software or code have been included and no new data were generated or analysed as part of this review.

References

1 B. Xu, S. Liu, J. L. Zhou, C. Zheng, J. Weifeng, B. Chen, T. Zhang and W. Qiu, *J. Hazard. Mater.*, 2021, **412**, 125159.
2 C. A. McDonough, S. Choyke, K. E. Barton, S. Mass, A. P. Starling, J. L. Adgate and C. P. Higgins, *Environ. Sci. Technol.*, 2021, **55**, 8139–8148.
3 U.S. Environmental Protection Agency, *PFAS National Primary Drinking Water Regulation*, Report EPA 815-F-24-003, 2024.
4 E. M. Sunderland, X. C. Hu, C. Dassuncao, A. K. Tokranov, C. C. Wagner and J. G. Allen, *J. Exposure Sci. Environ. Epidemiol.*, 2019, **29**, 131–147.
5 E. Panieri, K. Baralic, D. Djukic-Cosic, A. Buha Djordjevic and L. Saso, *Toxics*, 2022, **10**, 44.
6 A. Seyoum, A. Pradhan, J. Jass and P.-E. Olsson, *Sci. Total Environ.*, 2020, **737**, 139682.
7 K. R. Miner, H. Clifford, T. Taruscio, M. Potocki, G. Solomon, M. Ritari, I. E. Napper, A. P. Gajurel and P. A. Mayewski, *Sci. Total Environ.*, 2021, **759**, 144421.
8 A. J. Lewis, T. Joyce, M. Hadaya, F. Ebrahimi, I. Dragiev, N. Giardetti, J. Yang, G. Fridman, A. Rabinovich and A. A. Fridman, *Environ. Sci.:Water Res. Technol.*, 2020, **6**, 1044–1057.
9 Z. Wang, J. C. DeWitt, C. P. Higgins and I. T. Cousins, *Environ. Sci. Technol.*, 2017, **51**, 2508–2518.
10 A. Podder, A. H. M. A. Sadmani, D. Reinhart, N.-B. Chang and R. Goel, *J. Hazard. Mater.*, 2021, **419**, 126361.
11 J. Glüge, M. Scheringer, I. T. Cousins, J. C. DeWitt, G. Goldenman, D. Herzke, R. Lohmann, C. A. Ng, X. Trier and Z. Wang, *Environ. Sci.: Processes Impacts*, 2020, **22**, 2345–2373.
12 A. J. Williams, C. M. Grulke, J. Edwards, A. D. McEachran, K. Mansouri, N. C. Baker, G. Patlewicz, I. Shah, J. F. Wambaugh and R. S. Judson, *J. Cheminf.*, 2017, **9**, 1–27.
13 R. F. Menger, E. Funk, C. S. Henry and T. Borch, *Chem. Eng. J.*, 2021, **417**, 129133.
14 H. Chen, X. Wang, C. Zhang, R. Sun, J. Han, G. Han, W. Yang and X. He, *Environ. Pollut.*, 2017, **221**, 234–243.
15 R. C. Buck, J. Franklin, U. Berger, J. M. Conder, I. T. Cousins, P. de Voogt, A. A. Jensen, K. Kannan, S. A. Mabury and S. P. van Leeuwen, *Integr. Environ. Assess. Manage.*, 2011, **7**, 513–541.
16 J. L. Guelfo and C. P. Higgins, *Environ. Sci. Technol.*, 2013, **47**, 4164–4171.
17 S. E. Fenton, A. Ducatman, A. Boobis, J. C. DeWitt, C. Lau, C. Ng, J. S. Smith and S. M. Roberts, *Environ. Toxicol. Chem.*, 2020, **40**, 606–630.
18 A. M. Narizzano, E. M. Lent, J. M. Hanson, A. G. East, M. E. Bohannon and M. J. Quinn, *Reprod. Toxicol.*, 2022, **113**, 120–127.
19 T. Ma, P. Wu, L. Wang, Q. Li, X. Li and Y. Luo, *Front. Environ. Sci.*, 2023, **11**, 2023.
20 D. Savoca and A. Pace, *Int. J. Mol. Sci.*, 2021, **22**, 6276.
21 J. Wang, Z. Wang, Y. Tang, Y. Zhao, H. Fang, Y. Zhang, X. Hou, H. Tan, S. Yu, H. Zhang, H. Fan, T. Yang and S. Zhang, *ACS Omega*, 2024, **9**, 25370–25380.
22 C. M. Boston, N. Banacos and W. Heiger-Bernays, *Public Health Rep.*, 2019, **134**, 112–117.
23 C. F. Kwiatkowski, D. Q. Andrews, L. S. Birnbaum, T. A. Bruton, J. C. DeWitt, D. R. Knappe, M. V. Maffini, M. F. Miller, K. E. Pelch and A. Reade, *Environ. Sci. Technol. Lett.*, 2020, **7**, 532–543.
24 Agency for Toxic Substances and Disease Registry, *Toxicological Profile for Perfluoroalkyls*, U.S. Department of Health and Human Services, Public Health Service, Atlanta, GA, 2021.

25 United Nations Environment Programme, *Listing of Perfluorohexane Sulfonic Acid (PFHxS), its Salts and PFHxS-Related Compounds, Report Decision SC-10/13, Stockholm Convention on Persistent Organic Pollutants*, 2022.
26 A. Cordner, V. Y. De La Rosa, L. A. Schaider, R. A. Rudel, L. Richter and P. Brown, *J. Exposure Sci. Environ. Epidemiol.*, 2019, **29**, 157–171.
27 E. M. Bell, S. De Guise, J. R. McCutcheon, Y. Lei, M. Levin, B. Li, J. F. Rusling, D. A. Lawrence, J. M. Cavallari and C. O'Connell, *Sci. Total Environ.*, 2021, **780**, 146399.
28 S. F. Nakayama, M. Yoshikane, Y. Onoda, Y. Nishihama, M. Iwai-Shimada, M. Takagi, Y. Kobayashi and T. Isobe, *TrAC, Trends Anal. Chem.*, 2019, **121**, 115410.
29 J. A. Shoemaker, B. Boutin and P. Grimmett, *J. Chromatogr. Sci.*, 2009, **47**, 3–11.
30 L. J. Winchell, M. J. Wells, J. J. Ross, X. Fonoll, J. W. Norton Jr, S. Kuplicki, M. Khan and K. Y. Bell, *Sci. Total Environ.*, 2021, **774**, 145257.
31 U.S. Environmental Protection Agency, *Method 533: Determination of Per- and Polyfluoroalkyl Substances in Drinking Water by Isotope Dilution Anion Exchange Solid Phase Extraction and Liquid Chromatography/Tandem Mass Spectrometry*, Report EPA 815-B-19-020, 2019.
32 P. M. Choi, B. J. Tscharke, E. Donner, J. W. O'Brien, S. C. Grant, S. L. Kaserzon, R. Mackie, E. O'Malley, N. D. Crosbie and K. V. Thomas, *TrAC, Trends Anal. Chem.*, 2018, **105**, 453–469.
33 M. Al Amin, Z. Sobhani, Y. Liu, R. Dharmaraja, S. Chadalavada, R. Naidu, J. M. Chalker and C. Fang, *Environ. Technol. Innovation*, 2020, **19**, 100879.
34 J. John, F. Coulon and P. V. Chellam, *J. Water Process Eng.*, 2022, **45**, 102463.
35 J. Rodriguez-Perez, C. Leigh, B. Liquet, C. Kermorvant, E. Peterson, D. Sous and K. Mengersen, *Environ. Sci. Technol.*, 2020, **54**, 13719–13730.
36 S. R. Tatiparthi, Y. G. De Costa, C. N. Whittaker, S. Hu, Z. Yuan, R. Y. Zhong and W.-Q. Zhuang, *Water Res.*, 2021, **198**, 117107.
37 L. Gobelius, J. Hedlund, W. Dürig, R. Tröger, K. Lilja, K. Wiberg and L. Ahrens, *Environ. Sci. Technol.*, 2018, **52**, 4340–4349.
38 K. L. Rodriguez, J.-H. Hwang, A. R. Esfahani, A. Sadmani and W. H. Lee, *Micromachines*, 2020, **11**, 667.
39 S. J. Chow, N. Ojeda, J. G. Jacangelo and K. J. Schwab, *Water Res.*, 2021, **201**, 117292.
40 US-EPA, https://www.epa.gov/pfas/epa-pfas-drinking-water-laboratory-methods, 2025.
41 G. S. Frederick and O. Schmitz, *LCGC Supplements*, 2025, **23**, 20–25.
42 H. M. Sabatini, T. Pettit-Bacovin, R. Aderorho and C. D. Chouinard, *Anal. Chem.*, 2025, **97**, 6727–6734.
43 G. Munoz, P. Ray, S. Mejia-Avendaño, S. V. Duy, D. T. Do, J. Liu and S. Sauvé, *Anal. Chim. Acta*, 2018, **1034**, 74–84.
44 T. L. Coggan, T. Anumol, J. Pyke, J. Shimeta and B. O. Clarke, *Anal. Bioanal. Chem.*, 2019, **411**, 3507–3520.
45 R. G. de Vega, A. Cameron, D. Clases, T. M. Dodgen, P. A. Doble and D. P. Bishop, *J. Chromatogr. A*, 2021, **1653**, 462423.
46 L. W. Yeung, C. Stadey and S. A. Mabury, *J. Chromatogr. A*, 2017, **1522**, 78–85.
47 K. A. Barzen-Hanson and J. A. Field, *Environ. Sci. Technol. Lett.*, 2015, **2**, 95–99.
48 V. Mulabagal, L. Liu, J. Qi, C. Wilson and J. S. Hayworth, *Talanta*, 2018, **190**, 95–102.
49 A. A. Olomukoro, R. V. Emmons, N. H. Godage, E. Cudjoe and E. Gionfriddo, *J. Chromatogr. A*, 2021, **1651**, 462335.
50 W. J. Backe, T. C. Day and J. A. Field, *Environ. Sci. Technol.*, 2013, **47**, 5226–5234.
51 K. A. Barzen-Hanson, S. C. Roberts, S. Choyke, K. Oetjen, A. McAlees, N. Riddell, R. McCrindle, P. L. Ferguson, C. P. Higgins and J. A. Field, *Environ. Sci. Technol.*, 2017, **51**, 2047–2057.
52 F. Li, H. Huang, Z. Xu, H. Ni, H. Yan, R. Chen, Y. Luo, W. Pan, J. Long and X. Ye, *Bull. Environ. Contam. Toxicol.*, 2017, **99**, 760–764.
53 V. Boiteux, X. Dauchy, C. Rosin and J.-F. Munoz, *Arch. Environ. Contam. Toxicol.*, 2012, **63**, 1–12.
54 C. Chen, J. Wang, S. Yang, Z. Yan, Q. Cai and S. Yao, *Talanta*, 2013, **114**, 11–16.
55 C. Chen, X. Liang, J. Wang, Y. Zou, H. Hu, Q. Cai and S. Yao, *J. Chromatogr. A*, 2014, **1348**, 80–86.
56 J. Deng, Y. Yang, L. Fang, L. Lin, H. Zhou and T. Luan, *Anal. Chem.*, 2014, **86**, 11159–11166.
57 M. Filipovic, H. Laudon, M. S. McLachlan and U. Berger, *Environ. Sci. Technol.*, 2015, **49**, 12127–12135.
58 C. Bach, V. Boiteux, J. Hemard, A. Colin, C. Rosin, J.-F. Munoz and X. Dauchy, *J. Chromatogr. A*, 2016, **1448**, 98–106.
59 C.-G. Pan, Y.-S. Liu and G.-G. Ying, *Water Res.*, 2016, **106**, 562–570.
60 R. Loos, S. Tavazzi, G. Mariani, G. Suurkuusk, B. Paracchini and G. Umlauf, *Sci. Total Environ.*, 2017, **607**, 1201–1212.
61 V. Boiteux, X. Dauchy, C. Bach, A. Colin, J. Hemard, V. Sagres, C. Rosin and J.-F. Munoz, *Sci. Total Environ.*, 2017, **583**, 393–400.
62 Y.-C. Lee, P.-Y. Wang, S.-L. Lo and C. Huang, *Sep. Purif. Technol.*, 2017, **173**, 280–285.
63 J. Wang, Y. Shi and Y. Cai, *J. Chromatogr. A*, 2018, **1544**, 1–7.
64 Y. Huang, H. Li, M. Bai and X. Huang, *Anal. Chim. Acta*, 2018, **1011**, 50–58.
65 Z.-H. Deng, C.-G. Cheng, X.-L. Wang, S.-H. Shi, M.-L. Wang and R.-S. Zhao, *Molecules*, 2018, **23**, 902.
66 S. X. L. Goh and H. K. Lee, *Anal. Chim. Acta*, 2018, **1019**, 74–83.
67 H. A. Kaboré, S. V. Duy, G. Munoz, L. Méité, M. Desrosiers, J. Liu, T. K. Sory and S. Sauvé, *Sci. Total Environ.*, 2018, **616**, 1089–1100.
68 J. Shoemaker and D. Tettenhorst, *Method 537.1: Determination of Selected Per- and Polyfluorinated Alkyl Substances in Drinking Water by Solid Phase Extraction and Liquid Chromatography/Tandem Mass Spectrometry (LC/MS/MS)*, U.S. Environmental Protection Agency, Office of

Research and Development, National Center for Environmental Assessment, Washington, DC, 2018.
69 C. Wei, Q. Wang, X. Song, X. Chen, R. Fan, D. Ding and Y. Liu, *Ecotoxicol. Environ. Saf.*, 2018, **152**, 141–150.
70 J. F. Ayala-Cabrera, F. Javier Santos and E. Moyano, *Anal. Bioanal. Chem.*, 2018, **410**, 4913–4924.
71 J. Janda, K. Nödler, H.-J. Brauch, C. Zwiener and F. T. Lange, *Environ. Sci. Pollut. Res.*, 2019, **26**, 7326–7336.
72 T. E. Lockwood, M. Talebi, A. Minett, S. Mills, P. A. Doble and D. P. Bishop, *J. Chromatogr. A*, 2019, **1604**, 460495.
73 P. Suwannakot, F. Lisi, E. Ahmed, K. Liang, R. Babarao, J. J. Gooding and W. A. Donald, *Anal. Chem.*, 2020, **92**, 6900–6908.
74 O. S. Ahmad, T. S. Bedwell, C. Esen, A. Garcia-Cruz and S. A. Piletsky, *Trends Biotechnol.*, 2019, **37**, 294–309.
75 S. Ganesan, C. Chawengkijwanich, M. Gopalakrishnan and D. Janjaroen, *Food Chem. Toxicol.*, 2022, **168**, 113377.
76 Y. Jin and A. Granville, *J. Biosens. Bioelectron.*, 2016, **7**, 1–11.
77 Y. Wang, S. B. Darling and J. Chen, *ACS Appl. Mater. Interfaces*, 2021, **13**, 60789–60814.
78 C.-A. Bunge, M. Beckers and T. Gries, *Polymer Optical Fibres: Fibre Types, Materials, Fabrication, Characterisation and Applications*, Woodhead Publishing, 2016.
79 N. Sabri, S. A. Aljunid, M. S. Salim and S. Fouad, in *Recent Trends in Physics of Material Science and Technology*, ed. F. L. Gaol, K. Shrivastava and J. Akhtar, Springer Singapore, Singapore, 2015, pp. 299–311, DOI: 10.1007/978-981-287-128-2_19.
80 N. Cennamo, G. D'Agostino, G. Porto, A. Biasiolo, C. Perri, F. Arcadio and L. Zeni, *Sensors*, 2018, **18**, 1836.
81 N. Cennamo, G. D'Agostino, F. Sequeira, F. Mattiello, G. Porto, A. Biasiolo, R. Nogueira, L. Bilro and L. Zeni, *Sensors*, 2018, **18**, 3009.
82 N. Cennamo, L. Zeni, P. Tortora, M. E. Regonesi, A. Giusti, M. Staiano, S. D'Auria and A. Varriale, *Talanta*, 2018, **178**, 955–961.
83 N. Cennamo, F. Arcadio, C. Perri, L. Zeni, F. Sequeira, L. Bilro, R. Nogueira, G. D'Agostino, G. Porto and A. Biasiolo, 2019.
84 F. Faiz, G. Baxter, S. Collins, F. Sidiroglou and M. Cran, *Sens. Actuators, B*, 2020, **312**, 128006.
85 L. Yu, Z. Song, J. Peng, M. Yang, H. Zhi and H. He, *TrAC, Trends Anal. Chem.*, 2020, **127**, 115880.
86 G. G. Morbioli, T. Mazzu-Nascimento, A. M. Stockton and E. Carrilho, *Anal. Chim. Acta*, 2017, **970**, 1–22.
87 A. Manayil Parambil, E. Priyadarshini, S. Paul, A. Bakandritsos, V. K. Sharma and R. Zbořil, *J. Mater. Chem. A*, 2025, **13**, 8246–8281.
88 M. Al Amin, Z. Sobhani, S. Chadalavada, R. Naidu and C. Fang, *Environ. Technol. Innovation*, 2020, **18**, 100778.
89 S. Mahpishanian, M. Zhou and R. Foudazi, *Environ. Sci.:Adv.*, 2024, **3**, 1698–1713.
90 S. Garg, P. Kumar, G. W. Greene, V. Mishra, D. Avisar, R. S. Sharma and L. F. Dumée, *J. Environ. Manage.*, 2022, **308**, 114655.
91 J. Liu, J. Du, Y. Su and H. Zhao, *Microchem. J.*, 2019, **149**, 104019.
92 H. Niu, S. Wang, Z. Zhou, Y. Ma, X. Ma and Y. Cai, *Anal. Chem.*, 2014, **86**, 4170–4177.
93 C. Fang, X. Zhang, Z. Dong, L. Wang, M. Megharaj and R. Naidu, *Chemosphere*, 2018, **191**, 381–388.
94 Q. Chen, P. Zhu, J. Xiong, L. Gao and K. Tan, *Spectrochim. Acta, Part A*, 2020, **224**, 117362.
95 J. He, P. Qiu, J. Song, S. Zhang and Y. Bai, *Anal. Bioanal. Chem.*, 2020, **412**, 5329–5339.
96 M. K. Chini, V. Kumar, B. Maiti, P. De and S. Satapathi, *Polym. Test.*, 2019, **79**, 105997.
97 J. Park, K.-A. Yang, Y. Choi and J. K. Choe, *Environ. Int.*, 2022, **158**, 107000.
98 J. Park, D. Kim, D. Kim, J. Jung, K.-D. Zoh, C. Lee, Y. Choi and J. K. Choe, *Environ. Sci. Technol.*, 2025, **59**, 17247–17257.
99 H. Ryu, B. Li, S. De Guise, J. McCutcheon and Y. Lei, *J. Hazard. Mater.*, 2021, **408**, 124437.
100 M. Sgroi, E. Gagliano, F. G. A. Vagliasindi and P. Roccaro, *Sci. Total Environ.*, 2020, **711**, 134663.
101 Q. Liu, A. Huang, N. Wang, G. Zheng and L. Zhu, *J. Lumin.*, 2015, **161**, 374–381.
102 Q. Chen, P. Zhu, J. Xiong, L. Gao and K. Tan, *Microchem. J.*, 2019, **145**, 388–396.
103 Z. Cheng, H. Dong, J. Liang, F. Zhang, X. Chen, L. Du and K. Tan, *Spectrochim. Acta, Part A*, 2019, **207**, 262–269.
104 J. He, Y. Su, Z. Sun, R. Zhang, F. Wu and Y. Bai, *Microchem. J.*, 2020, **157**, 105030.
105 L. Lin, S. Zhou, H. Guo, Y. Chen, S. Lin, L. Yan, K. Li and J. Li, *Microchim. Acta*, 2019, **186**, 1–9.
106 Z. Cheng, L. Du, P. Zhu, Q. Chen and K. Tan, *Spectrochim. Acta, Part A*, 2018, **201**, 281–287.
107 Y. Wang and H. Zhu, *Anal. Methods*, 2014, **6**, 2379–2383.
108 L. S. Walekar, M. Zheng, L. Zheng and M. Long, *Microchim. Acta*, 2019, **186**, 278.
109 M. Yin, L. Che, S. Jiang, Q. Deng and S. Wang, *Environ. Sci.: Nano*, 2020, **7**, 3036–3046.
110 L. Tian, H. Guo, J. Li, L. Yan, E. Zhu, X. Liu and K. Li, *J. Hazard. Mater.*, 2021, **413**, 125353.
111 H. Feng, N. Wang, L. Yuan, J. Li and Q. Cai, *Sens. Actuators, B*, 2014, **195**, 266–273.
112 L. Zheng, Y. Zheng, Y. Liu, S. Long, L. Du, J. Liang, C. Huang, M. T. Swihart and K. Tan, *Talanta*, 2019, **194**, 1–6.
113 C. Fang, J. Wu, Z. Sobhani, M. Al Amin and Y. Tang, *Anal. Methods*, 2019, **11**, 163–170.
114 J. Liang, X. Deng and K. Tan, *Spectrochim. Acta, Part A*, 2015, **150**, 772–777.
115 S.-N. Lei and H. Cong, *Chin. Chem. Lett.*, 2022, **33**, 1493–1496.
116 Z. Fredj and M. Sawan, *Biosensors*, 2023, **13**, 211.
117 Y. Zheng, X. Song, Z. Fredj, S. Bian and M. Sawan, *Anal. Chim. Acta*, 2023, **1244**, 340860.
118 Z. Fredj, P. Wang, F. Ullah and M. Sawan, *Microchim. Acta*, 2023, **190**, 343.
119 M. H. Hassan, R. Khan and S. Andreescu, *Electrochem. Sci. Adv.*, 2022, **2**, e2100184.

120 M. W. Glasscott, K. J. Vannoy, R. Kazemi, M. D. Verber and J. E. Dick, *Environ. Sci. Technol. Lett.*, 2020, **7**, 489–495.
121 N. Karimian, A. M. Stortini, L. M. Moretto, C. Costantino, S. Bogialli and P. Ugo, *ACS Sens.*, 2018, **3**, 1291–1298.
122 R. B. Clark and J. E. Dick, *ACS Sens.*, 2020, **5**, 3591–3598.
123 S. Chen, A. Li, L. Zhang and J. Gong, *Anal. Chim. Acta*, 2015, **896**, 68–77.
124 T. Tran.T, J. Li, H. Feng, J. Cai, L. Yuan, N. Wang and Q. Cai, *Sens. Actuators, B*, 2014, **190**, 745–751.
125 C. Fang, Z. Chen, M. Megharaj and R. Naidu, *Environ. Technol. Innovation*, 2016, **5**, 52–59.
126 X. Li, X. Wang, T. Fang, L. Zhang and J. Gong, *Talanta*, 2018, **181**, 147–153.
127 G. Moro, F. Bottari, S. Liberi, S. Covaceuszach, A. Cassetta, A. Angelini, K. De Wael and L. M. Moretto, *Bioelectrochemistry*, 2020, **134**, 107540.
128 R. He, L. Zhao, W. Yan, Y. Guo, C. Dong and L. Fan, *ACS Sens.*, 2025, **10**, 3746–3756.
129 T. Zhang, H. Zhao, A. Lei and X. Quan, *Electrochemistry*, 2014, **82**, 94–99.
130 Z. Meng, R. M. Stolz, L. Mendecki and K. A. Mirica, *Chem. Rev.*, 2019, **119**, 478–598.
131 V. Chugh, P. Gaskin and W. Zhang, *Sens. Diagn.*, 2026, **5**, 305–325.
132 R. Ranaweera, C. Ghafari and L. Luo, *Anal. Chem.*, 2019, **91**, 7744–7748.
133 V. Kesler, B. Murmann and H. T. Soh, *ACS Nano*, 2020, **14**, 16194–16201.
134 J. Dai and M. Fidalgo de Cortalezzi, *Heliyon*, 2019, **5**, e01922.
135 J. E. Contreras-Naranjo and O. Aguilar, *Biosensors*, 2019, **9**, 15.
136 J. J. BelBruno, *Chem. Rev.*, 2018, **119**, 94–119.
137 A. H. Karoyo and L. D. Wilson, *J. Colloid Interface Sci.*, 2013, **402**, 196–203.
138 A. A. Lahcen and A. Amine, *Electroanalysis*, 2019, **31**, 188–201.
139 G. Moro, D. Cristofori, F. Bottari, E. Cattaruzza, K. De Wael and L. M. Moretto, *Sensors*, 2019, **19**, 4433.
140 J. Gong, T. Fang, D. Peng, A. Li and L. Zhang, *Biosens. Bioelectron.*, 2015, **73**, 256–263.
141 R. Kazemi, E. I. Potts and J. E. Dick, *Anal. Chem.*, 2020, **92**, 10597–10605.
142 B. Manivannan, G. Nallathambi and T. Devasena, *Environ. Sci.: Processes Impacts*, 2022, **24**, 2009–2031.
143 N. Gondhiya, A. U. Rehman, D. Andreescu and S. Andreescu, *Curr. Opin. Electrochem.*, 2025, **53**, 101725.
144 L. Wójcik, B. Szostek, W. Maruszak and M. Trojanowicz, *Electrophoresis*, 2005, **26**, 1080–1088.
145 L. Wójcik, K. Korczak, B. Szostek and M. Trojanowicz, *J. Chromatogr. A*, 2006, **1128**, 290–297.
146 D.-S. Lian, S.-J. Zhao, J. Li and B.-L. Li, *Anal. Bioanal. Chem.*, 2014, **406**, 6129–6150.
147 R. Knob, V. Maier, J. Petr, V. Ranc and J. Ševčík, *Electrophoresis*, 2012, **33**, 2159–2166.
148 H. Lees, P. Jõul, K. Siilak and M. Vaher, *Sep. Sci. plus*, 2020, **3**, 313–320.
149 O. Höcker, T. Bader, T. C. Schmidt, W. Schulz and C. Neusüß, *Anal. Bioanal. Chem.*, 2020, **412**, 4857–4865.
150 S. Azab, R. Hum and P. Britz-McKibbin, *Anal. Sci. Adv.*, 2020, **1**, 173–182.
151 M. Zhang, Y. Zhao, B. Bui, L. Tang, J. Xue, M. Chen and W. Chen, *Crit. Rev. Anal. Chem.*, 2025, **55**, 542–558.
152 R. B. Clark and J. E. Dick, *Chem. Commun.*, 2021, **57**, 8121–8130.
153 S. Yaghoobian, M. A. Ramirez-Ubillus, L. Zhai and J.-H. Hwang, *Chem. Sci.*, 2025, **16**, 13564–13573.
154 M. Takayose, K. Akamatsu, H. Nawafune, T. Murashima and J. Matsui, *Anal. Lett.*, 2012, **45**, 2856–2864.
155 D. A. Bellido-Aguilar, M. Dunmyer, C. S. Malloy, M. J. Danley, V. Karanikola and S. Savagatrup, *RSC Adv.*, 2025, **15**, 20341–20349.
156 K. Kannan, *Environ. Health Perspect.*, 2025, **133**, 011301.
157 G. K. Ali and K. M. Omer, *Talanta*, 2022, **236**, 122878.
158 P. Aryal, C. Hefner, B. Martinez and C. S. Henry, *Lab Chip*, 2024, **24**, 1175–1206.
159 E. El-Shafeiy, M. Alsabaan, M. I. Ibrahem and H. Elwahsh, *Sensors*, 2023, **23**, 8613.
160 H. Medina and C. Farmer, *Toxics*, 2024, **12**, 610.
161 D. Quintana, L. C. Felix-Herran, J. C. Tudon-Martinez and J. d. J. Lozoya-Santos, *Water*, 2025, **17**, 2571.
162 D. Thompson, N. Zolfigol, Z. Xia and Y. Lei, *Sens. Actuators Rep.*, 2024, **7**, 100189.